Edinburgh Research Explorer

Neutral kaon mixing beyond the Standard Model with nf=2+1 chiral fermions part II

Citation for published version:
Boyle, PA, Garron, N, J. Hudspith, R, Lehner, C & Lytle, AT 2017, 'Neutral kaon mixing beyond the Standard Model with nf=2+1 chiral fermions part II: Non Perturbative Renormalisation of the F=2 four-quark operators', *Journal of High Energy Physics*, vol. 10, no. 054. https://doi.org/10.1007/JHEP10(2017)054

Digital Object Identifier (DOI):
10.1007/JHEP10(2017)054

Link:
Link to publication record in Edinburgh Research Explorer

Document Version:
Publisher's PDF, also known as Version of record

Published In:
Journal of High Energy Physics

OPEN ACCESS

Download date: 04. Jan. 2021

Neutral kaon mixing beyond the Standard Model with $n_f = 2+1$ chiral fermions part II: Non Perturbative Renormalisation of the $\Delta F = 2$ four-quark operators

P.A. Boyle [1], N. Garron [2a], R.J. Hudspith [3], C. Lehner [4], A.T. Lytle [5].

[1] *Higgs Centre for Theoretical Physics, School of Physics & Astronomy,*
University of Edinburgh, EH9 3FD, UK,

[2] *Theoretical Physics Division, Department of Mathematical Sciences,*
University of Liverpool, Liverpool L69 3BX, UK,

[3] *Department of Physics and Astronomy, York University, Toronto, Ontario, M3J 1P3, Canada,*

[4] *Physics Department, Brookhaven National Laboratory, Upton, NY 11973, USA, and*

[5] *SUPA, School of Physics and Astronomy, University of Glasgow, Glasgow, G12 8QQ, UK.*

(The RBC and UKQCD collaborations)

(Dated: August 14, 2017)

We compute the renormalisation factors (Z-matrices) of the $\Delta F = 2$ four-quark operators needed for Beyond the Standard Model (BSM) kaon mixing. We work with $n_f = 2+1$ flavours of Domain-Wall fermions whose chiral-flavour properties are essential to maintain a continuum-like mixing pattern. We introduce new RI-SMOM renormalisation schemes, which we argue are better behaved compared to the commonly-used corresponding RI-MOM one. We find that, once converted to $\overline{\text{MS}}$, the Z-factors computed through these RI-SMOM schemes are in good agreement but differ significantly from the ones computed through the RI-MOM scheme. The RI-SMOM Z-factors presented here have been used to compute the BSM neutral kaon mixing matrix elements in the companion paper [1]. We argue that the renormalisation procedure is responsible for the discrepancies observed by different collaborations, we will investigate and elucidate the origin of these differences throughout this work.

[a] nicolas.garron@liverpool.ac.uk

I. INTRODUCTION

Numerical simulations of Quantum ChromoDynamics (QCD) allow for first-principle evaluations of hadronic matrix elements, which play a crucial rôle in theoretical calculations as they encapsulate the low-energy physics of a process. Computation of such matrix elements is usually done in two steps: Firstly, the bare quantities of interest are computed at finite lattice spacing a, whose inverse plays the rôle an ultra-violet regulator. Secondly, these quantities have to be renormalised in order to be divergence-free and have a well-defined continuum limit ($a^2 \to 0$). There are two known non-perturbative methods to perform this renormalisation: the Schrödinger Functional (SF) scheme and the other being the Rome-Southampton method [2]. We choose to work with the latter, for practical reasons (the interested reader can find a recent study of the same set of operators within the SF in [3] and [4]). In phenomenological applications the renormalised quantities are then matched to a scheme in which the corresponding short distance contributions can be computed, this is commonly performed in the modified minimal subtraction scheme $\overline{\rm MS}$, see for example [5, 6].

Let us begin by considering the matrix element of an operator $\langle O \rangle$ which renormalises multiplicatively, and with $\langle O \rangle^{\rm bare}(a)$ being a bare matrix element computed at finite lattice spacing a. We denote $Z^{\rm RI}$ the corresponding renormalisation factor computed on the same lattice (following the Rome-Southampton method) in a regularisation independent (RI) scheme. The precise definition of the schemes (RI-MOM or a RI-SMOM) will be given in the next section. Within our conventions, at some renormalisation scale μ, the renormalised matrix element is given by

$$\langle O \rangle^{\rm RI}(\mu, a) = Z^{\rm RI}(\mu, a)\langle O \rangle^{\rm bare}(a) \;, \tag{1}$$

which now has a well defined continuum limit

$$\langle O \rangle^{\rm RI}(\mu) = \lim_{a^2 \to 0} \langle O \rangle^{\rm RI}(\mu, a) \;. \tag{2}$$

Suppose now that this operator occurs in the determination of some physical quantity, say an amplitude. For example in a typical phenomenological application the hadronic matrix element has to be combined with a Wilson coefficient $C(\mu)$ computed in continuum perturbation theory (the hadronic matrix element describes the long-distance effetcts and the Wilson coefficient the short-distance ones). Both of these must be computed in a common scheme, $\overline{\rm MS}$, to be matched

to a physical quantity. Schematically we have

$$
\begin{aligned}
\text{Amplitude} &= C^{\overline{\text{MS}}}(\mu)\langle O\rangle^{\overline{\text{MS}}}(\mu) \ , \\
&= C^{\overline{\text{MS}}}(\mu)R^{\overline{\text{MS}}\leftarrow\text{RI}}(\mu)\langle O\rangle^{\text{RI}}(\mu) \ , \\
&= C^{\overline{\text{MS}}}(\mu)R^{\overline{\text{MS}}\leftarrow\text{RI}}(\mu)\lim_{a^2\to 0}\left[Z^{\text{RI}}(\mu,a)\langle O\rangle^{bare}(a)\right] \ ,
\end{aligned}
\tag{3}
$$

where R is the conversion factor from the RI scheme to $\overline{\text{MS}}$. Eq. 3 can easily be generalised to the operator mixing case where $\langle O\rangle$ and C become vectors, and R and Z become matrices. We remind the reader that although the renormalisation is performed non-perturbatively, the matching to $\overline{\text{MS}}$ from the RI scheme ($R^{\overline{\text{MS}}\leftarrow\text{RI}}(\mu)$) has to be done using continuum perturbation theory as $\overline{\text{MS}}$ is not possible to implement on the lattice.

Accurate matching of lattice operators using the Rome-Southampton technique requires the matching scale μ (given by the magnitude of a momentum $\mu = \sqrt{p^2}$) to be well-separated from both the scales where non-perturbative effects of QCD such as chiral symmetry-breaking become important and the (inverse) lattice scale where cut-off effects dominate; ideally one would impose

$$
\Lambda_{\text{QCD}}^2 \ll \mu^2 \ll \left(\frac{\pi}{a}\right)^2 .
\tag{4}
$$

The first condition ensures that a perturbative treatment of the matching to $\overline{\text{MS}}$ is justified, while the latter ensures that the lattice artifacts are under control [1]. The $\overline{\text{MS}}$ renormalisation factors should be independent of the intermediate (RI) scheme used; however, in practice there will be some dependence due to systematic uncertainties in the lattice matching step as well as perturbative truncation errors in the continuum matching.

We compute the Z-matrix needed to renormalise the operators required for the determination of neutral kaon mixing beyond the Standard Model (BSM). As is usually done by the RBC-UKQCD collaboration, we implement momentum sources and partially-twisted boundary conditions. The use of momentum sources (introduced by QCDSF in [9]) results in very low statistical noise while the use of partially-twisted boundary conditions allows us to change $\mu = p^2$ smoothly while keeping the orientation of p fixed [10–12]. In this way we do not discontinuously 'jump' into different hypercubic representations as p^2 varies, resulting in Zs which are smooth functions of p^2.

In principle, after extrapolation to the continuum and conversion to $\overline{\text{MS}}$ (or any common scheme) at a given scale, the results should be universal - up to truncation error of the perturbative series - and in particular should not depend on the details of the discretisation. The physical results

---

[1] This restriction known at the Rome-Southampton window and can be relaxed with step-scaling methods [7, 8]

N_f	interm. scheme	R_4	R_5
2	RI-MOM	28.5(9)	7.3(4)
$2+1$	RI-MOM	34.6(22)	8.5(9)
$2+1$	(γ_μ, γ_μ)	43.1(25)	11.0(9)
$2+1$	$(\slashed{q}, \slashed{q})$	44.3(25)	10.7(9)

TABLE I. Example of results for the ratio of the BSM matrix elements over the SM one $R_i = \langle \bar{K}|O_i^{BSM}|K\rangle/\langle \bar{K}|O^{SM}K\rangle$, in $\overline{\text{MS}}$ at 3 GeV in the SUSY basis. The statistical and systematic errors have been combined in quadrature. Although in principle these quantities should agree up to α_s^2 errors, the RI-MOM results differ significantly from the (γ_μ, γ_μ) and $(\slashed{q}, \slashed{q})$ ones, which are consistent with each other. The latter are RI-SMOM schemes whose precise definitions are given in this work. The $N_f = 2+1$ results quoted here are obtained with exactly the same framework apart from the intermediate renormalisation scheme, see [1]. We argue that the difference comes the renormalisation and we suggest to discard the results obtained with the RI-MOM scheme. Not included are results obtained with $N_f = 2+1+1$ flavours by the ETM collaboration [13], which are roughly consistent with the $N_f = 2$ RI-MOM results, and by SWME with $N_f = 2+1$ [14, 15], which are in a good agreement with our RI-SMOM results, see text for discussion.

could still depend on the number of dynamical flavours but, by experience, we do not expect this dependence to be important for the weak matrix elements discussed in this work. In the past few years, these matrix elements have been computed by three different collaborations and some discrepancy has been observed for two of the four relevant four-quark operators. The first results with dynamical quarks was reported by our collaboration in [16], it was done with $N_f = 2+1$ flavours of dynamical quarks at a single value of the lattice spacing. Shortly after our work was published, the ETM collaboration published their study with $N_f = 2$ flavours and several lattice spacings [17], they found compatible results (within 2σ for O_5). Then the SWME collaboration [14] reported on their computation, using $N_f = 2+1$ flavours of improved staggered and again several lattice spacings. They find an important disagreement for two of these matrix elements. The ETM collaboration has then repeated their computation with $N_f = 2+1+1$ flavours [13] and found roughly the same results as in their previous study (again only within $\sim 2\sigma$ for O_5 and the new result is now in perfect agreement with our old result).

In [1, 18], we added another lattice spacing and investigated the origin of the discrepancy. In particular for the non-perturbative renormalisation procedure, in addition to the traditional RI-MOM scheme, we have implemented new intermediate renormalisation schemes, called (γ_μ, γ_μ) and $(\slashed{q}, \slashed{q})$ which satisfy the RI-SMOM condition, and therefore exhibit non-exceptional kinemat-

ics. As summarised in Table I, we find that the results depend significantly on the intermediate renormalisation scheme:

- If we use the traditional RI-MOM scheme with exceptional kinematics, we reproduce our old result and are compatible with ETMc, who used the same RI-MOM scheme .

- With the RI-SMOM schemes, our results for O_4 and O_5 are significantly different from our old RI-MOM results, but are consistent with each other.

- Our new RI-SMOM results are also in good agreement with SWME, who perform the renormalisation at one-loop in perturbation theory. This has been confirmed by the update of SWME [15]. Therefore, one of our main conclusions in [1, 18] is that the renormalisation procedure is the source of the discrepancy and we suggest to discard the results obtained with exceptional kinematics due to the systematic uncertainty in the pion pole subtraction.

In Table I, we choose to compare the results for R_i [19] as they give directly the deviation of new physics with respect to the SM contribution. Since we could not find these quantities in [13–15], we do not show the results from ETMc ($N_f = 2 + 1 + 1$) and SWME. However such a comparison for the bag parameters can be found in [1].

The main purpose of this work is the definition of RI-SMOM schemes for the BSM operators, generalising what has been done for the Standard Model B_K and for $K \to \pi\pi$ matrix elements [8, 20–27]. These RI-SMOM schemes use non-exceptional kinematics with a symmetric point and have much better infrared behaviour, resulting in the suppression of pion pole contribution and wrong-chirality operator mixing [28, 29]. We argue in this work that at this point, results obtained using the RI-MOM scheme should be approached with skepticism or, if possible even discarded, at least for these quantities (the renormalisation of BSM kaon mixing operators). In addition, we define two new NPR schemes which both have different perturbative truncation systematics, upon comparing the two we can cleanly estimate the systematic from the renormalisation procedure

The paper is organised as follows: in the next section we explain our procedure to obtain the Z factors. In Section III we give the explicit definitions of the projectors, which complete the definition of the schemes. The numerical results can be found in Section IV. In Section V we discuss the pole subtraction and the advantages of using the RI-SMOM schemes. Section VI contains our conclusions. Further details can be found in the appendices, where we give the relevant Z-factors for the bag parameters, the non-perturbative scale evolution of our renormalisation matrices, its

comparison with perturbation theory, and finally the Fierz relations for the operators considered here.

II. METHODOLOGY

The Non-Perturbative-Renormalization (NPR) procedure works as follows: we compute numerically the Landau-gauge-fixed Green's functions of the operators of interest between incoming and outgoing quarks in a given kinematic configuration. After amputation of the external legs, projection onto the Dirac-colour structure and extrapolation to the chiral limit, we require that the renormalised Green's functions are equal to their tree-level values. Since we renormalise a set of four-quark operators which can mix, this renormalisation condition defines a matrix of renormalisation factors. We will discuss importance of the choice of kinematics; in particular the renormalisation condition is imposed for a certain momentum transfer p which defines the renormalisation scale $\mu = \sqrt{p^2}$. For comparison we will also implement the original RI-MOM scheme [2], for which results at a single lattice spacing were presented in [16], but we chose to discard them for our final result in [1] as we will argue herein they appear to suffer from large systematic errors.

In the Standard Model only one operator contributes to neutral kaon mixing (a and b are colour indices)

$$Q_1 = (\bar{s}_a \gamma_\mu (1 - \gamma_5) d_a) (\bar{s}_b \gamma_\mu (1 - \gamma_5) d_b). \tag{5}$$

Beyond the Standard Model, under reasonable assumptions, four other four-quark operators are required (seven if parity is not conserved). Different choices of basis are possible but since we are concerned here with renormalisation, we find it convenient to only consider color-unmixed operators, i.e. those with the same colour structure as Q_1. In Appendix VII D we give the relation between the colour-mixed and colour-unmixed operators. In order to simplify the equations, we do not explicitly write the colour indices, the contraction over spin and colour indices is simply indicated by the parentheses. We define the BSM operators (see for example [5]):

$$
\begin{aligned}
Q_2 &= (\bar{s} \gamma_\mu (1 - \gamma_5) d) (\bar{s} \gamma_\mu (1 + \gamma_5) d), \\
Q_3 &= (\bar{s} (1 - \gamma_5) d) (\bar{s} (1 + \gamma_5) d), \\
Q_4 &= (\bar{s} (1 - \gamma_5) d) (\bar{s} (1 - \gamma_5) d), \\
Q_5 &= \frac{1}{4} (\bar{s} (\sigma_{\mu\nu} (1 - \gamma_5)) d) (\bar{s} (\sigma_{\mu\nu} (1 - \gamma_5)) d) .
\end{aligned}
\tag{6}
$$

where $\sigma_{\mu\nu} = \frac{1}{2}[\gamma_\mu, \gamma_\nu]$. In practice we only consider the parity-even part of these operators,

$$
\begin{aligned}
Q_1^+ &= (\overline{s}\gamma_\mu d)(\overline{s}\gamma_\mu d) + (\overline{s}\gamma_\mu\gamma_5 d)(\overline{s}\gamma_\mu\gamma_5 d), \\
Q_2^+ &= (\overline{s}\gamma_\mu d)(\overline{s}\gamma_\mu d) - (\overline{s}\gamma_\mu\gamma_5 d)(\overline{s}\gamma_\mu\gamma_5 d), \\
Q_3^+ &= (\overline{s}d)(\overline{s}d) - (\overline{s}\gamma_5 d)(\overline{s}\gamma_5 d), \\
Q_4^+ &= (\overline{s}d)(\overline{s}d) + (\overline{s}\gamma_5 d)(\overline{s}\gamma_5 d), \\
Q_5^+ &= \sum_{\nu > \mu} (\overline{s}\gamma_\mu\gamma_\nu d)(\overline{s}\gamma_\mu\gamma_\nu d).
\end{aligned}
\tag{7}
$$

We will refer to Eq. 7 as the NPR basis (the relation between the SUSY and the NPR basis can be found in Appendix VII D). The factor $1/4$ in Q_5 of Eq. (6) ensures that our definition matches the ususal lattice convention:

$$
\begin{aligned}
\sigma_{\mu\nu}(1 - \gamma_5) \times \sigma_{\mu\nu}(1 - \gamma_5) &= 2\sigma_{\mu\nu} \times \sigma_{\mu\nu} + \text{ parity odd terms} \\
&= 4\sum_{\nu > \mu} \gamma_\mu\gamma_\nu \times \gamma_\mu\gamma_\nu + \text{ parity odd terms}
\end{aligned}
\tag{8}
$$

These four-quark operators mix under renormalisation and - in a massless scheme - the mixing pattern is given by the chiral properties of these operators. They belong to three different representations of $SU_L(3) \times SU_R(3)$: It is well-known that the Standard Model operator Q_1 transforms as $(27, 1)$ and renormalises multiplicatively. Similarly, one can easily see that $Q_{2,3}$ transform like $(8, 8)$ while $Q_{4,5}$ transform like $(6, \overline{6})$.

If chiral symmetry were perfectly maintained in the lattice theory, the mixing pattern would consist solely of a single Z-factor for the $(27, 1)$ while the $(8, 8)$s and $(6, \overline{6})$s will each mix among themselves producing a block-diagonal structure with a single element in Z_{11} and two blocks of 2×2 mixing matrices in $Z_{2/3,2/3}$ and $Z_{4/5,4/5}$. Since the Domain-Wall action exhibits a continuum-like chiral-flavor symmetry (to a very good approximation), we expect to find a mixing pattern very close to the continuum one. However the effects of spontaneous chiral symmetry breaking will be present at some level and could introduce some forbidden mixing (mixing between operators which belong to different representations of $SU_L(3) \times SU_R(3)$). These unwanted infrared contaminations decrease as the renormalisation scale is increased beyond the typical interaction scale of QCD (Λ_{QCD}).

Such unphysical mixings are strongly suppressed in SMOM schemes (compared to the RI-MOM scheme), where the choice of kinematic prevents the contribution of exceptional momentum configurations [28]. In practice, we will take the degree to which the expected continuum mixing pattern is satisfied as a quantitative indicator of the degree to which the NPR condition Eq (4) is satisfied.

A.   Choice of kinematic and vertex functions

The choice of kinematic for the RI-SMOM schemes is illustrated in Fig. (1). There are two different momenta p_1 and p_2 such that the momentum transfer is $p^2 = (p_2 - p_1)^2$. In this way a single renormalisation scale $\mu = \sqrt{p^2}$ is maintained and momentum flows through the vertex, which suppresses unwanted non-perturbative behaviour compared to the original RI-MOM scheme [2]. In practice we need two (momentum source) propagators, we associate a momentum to a given flavour, here p_1 for the d-quark and p_2 for the s-quark. The momenta used are of the form (the Euclidian-time component is the last coordinate)

$$p_1 = \frac{2\pi}{L}(-m, 0, m, 0) \text{ and } p_2 = \frac{2\pi}{L}(0, m, m, 0) , \tag{9}$$

so that $p = p_2 - p_1 = \frac{2\pi}{L}(m, m, 0, 0)$. Since we use twisted boundary conditions in the valence sectors the momenta are not restricted to the Fourier modes. Our conventions are such that $m = n + \pi/2$, with $n \in \mathbb{Z}$ and $\theta \in \mathbb{R}$.

$$p = \frac{2\pi}{L}(-n, 0, n, 0) + \frac{\pi}{L}(-\theta, 0, \theta, 0) , \tag{10}$$

where θ is the twist angle of the boundary condition and n is an integer Fourier mode.

Our choice of convention is the following: with respect to the position of the vertex x,

1. An incoming s quark with momentum p_2 is denoted by

$$G_x(p_2) = \sum_y G^{(s)}(x, y) e^{ip_2.(y-x)} \tag{11}$$

2. An outgoing d quark with momentum $-p_1$ is denoted by

$$\bar{G}_x(p_1) = \gamma_5 G(x, p_1)^\dagger \gamma_5 = \sum_y e^{-ip_1.(y-x)} G^{(d)}(y, x) \tag{12}$$

For each operator Q_i of Eq.6 we compute the following Green's function (where we define $\tilde{x}_i = x_i - x$)

$$M_i^{\delta\gamma;\beta\alpha}(q^2) = \sum_{x,x_1,\ldots,x_4} \langle 0|s^\delta(x_4)\bar{d}^\gamma(x_3) [Q_i(x)] s^\beta(x_2)\bar{d}^\alpha(x_1)|0\rangle e^{-ip_1.\tilde{x}_1 + ip_2.\tilde{x}_2 - ip_1.\tilde{x}_3 + ip_2.\tilde{x}_4} ,$$

$$= 2 \sum_x \left(\langle \left[\bar{G}_x(p_2)\Gamma^1_{(i)}G_x(p_1)\right]^{\delta\gamma} \left[\bar{G}_x(p_2)\Gamma^2_{(i)}G_x(p_1)\right]^{\beta\alpha} \rangle \tag{13} \right.$$

$$\left. - \langle \left[\bar{G}_x(p_2)\Gamma^1_{(i)}G_x(p_1)\right]^{\delta\alpha} \left[\bar{G}_x(p_2)\Gamma^2_{(i)}G_x(p_1)\right]^{\beta\gamma} \rangle \right) ,$$

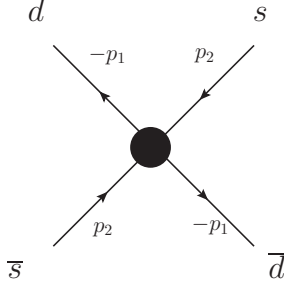[2] In the orginial RI-MOM scheme there is no momentum transfer $p_1 = p_2$.

FIG. 1. Illustration of the choice of kinematics in an RI-SMOM scheme for a four quark operator contributing to the process $(\bar{s}d) \to (\bar{d}s)$. We choose the momenta $p_1 \neq p_2$ such that $p_1^2 = p_2^2 = (p_1 - p_2)^2$. This configuration prevents the existence of a channel with zero-momentum transfer.

where the Greek letters denote combined spin-color indices. The color-Dirac structure of the four-quark operator Q_i is encoded in $\Gamma_{(i)}^{1,2}$, (there is no summation over i in Eq. 13). For the numerical implementation, we have only considered four-quark operators that are color unmixed (the color partners can be obtained by Fierz transformation, see Appendix VII D). For example, if i, j, k, l are Dirac indices and a, b, c, d are color indices, then for the operator Q_2, we have

$$(\Gamma^1)_{ij}^{ab} \times (\Gamma^2)_{kl}^{cd} = [\gamma_\mu(1 - \gamma_5)]_{ij} \, \delta^{ab} \times [\gamma_\mu(1 + \gamma_5)]_{kl} \, \delta^{cd} . \tag{14}$$

The vertex functions are then amputated

$$\Pi_i^{\bar{\delta}\bar{\gamma};\bar{\beta}\bar{\alpha}} = \langle \bar{G}(p_2)^{-1} \rangle^{\bar{\delta}\delta} \, \langle G(p_1)^{-1} \rangle^{\gamma\bar{\gamma}} \, \langle \bar{G}(p_2)^{-1} \rangle^{\bar{\beta}\beta} \, \langle G(p_1)^{-1} \rangle^{\alpha\bar{\alpha}} \, M_i^{\delta\gamma;\beta\alpha}(q^2), \tag{15}$$

where we have introduced the inverse of the "full momentum propagators"

$$G(p) = \sum_x G_x(p) \quad \text{and} \quad \bar{G}(p) = \sum_x \bar{G}_x(p) . \tag{16}$$

We still have to project these amputated vertex functions in order to obtain the renormalisation matrix. This is described in the next section.

B. Projection

Following Eq. 1, we introduce the renormalisation matrix Z which relates the renormalised four-quark operators to the bare ones (we drop the superscript RI for the Z factors)

$$\langle Q_i \rangle^{\text{RI}}(\mu, a) = Z_{ij}(\mu, a) \langle Q_j \rangle^{\text{bare}}(a), \tag{17}$$

Denoting by Π_i^{bare} the bare amputated Green's function of the four quark operator Q_i, the matrix Z_{ij} is defined by imposing the renormalisation condition [3]:

$$P_k \left[\frac{Z_{ij}(\mu, a)}{Z_q^2(\mu, a)} \Pi_j^{\text{bare}}(a, p^2) \right]_{p^2 = \mu^2} = F_{ik} ,\tag{18}$$

where $\sqrt{Z_q}$ is the quark wave function renormalisation. In the previous equation, P_i projects onto the tree-level spin-colour structure of Q_i:

$$P_k \left[\Pi_i^{(0)} \right] = F_{ik} ,\tag{19}$$

where the superscript (0) denotes the tree-level value. The fact that there is a non-vanishing momentum transfer in the vertex gives us more freedom for the choice of projectors. In this work, we introduce two different sets of projectors: $P^{(\gamma^\mu)}$ and $P^{(\not{q})}$, they are defined explicitly below. We also need a prescription for the quark wave function Z_q. This is done in two steps: first we cancel the factors of Z_q in (18) using the vertex function of the local vector current. The value of Z_V is then determined from some Ward identity in [30]. We implement two projectors $P_V^{(\gamma_\mu)}$ and $P_V^{(\not{q})}$ to obtain Z_V/Z_q. The choices of projectors for the four-quark operators and for the vector current define the non-perturbative scheme. Denoting by $\mathcal{A}$ and $\mathcal{B}$ the choices of projectors, ie (γ_μ) or $(\not{q})$, for both the four-quark operators and the vector current, the NPR condition for the scheme $(\mathcal{A}, \mathcal{B})$ reads

$$\frac{Z_{ij}^{(\mathcal{A}, \mathcal{B})}(\mu, a)}{Z_V(a)^2} \times \left. \frac{P_k^{\mathcal{A}} \left[\Pi_j^{bare}(a, p^2) \right]}{(P_V^{\mathcal{B}} \left[\Pi_V^{bare}(a, p^2) \right])^2} \right|_{p^2 = \mu^2} = \frac{F_{ik}^{\mathcal{A}}}{F_V^{\mathcal{B}}} .\tag{20}$$

The matrix $Z^{(\mathcal{A}, \mathcal{B})}$ converts the bare four-quark operators onto the renormalised four-quark operators in the RI-SMOM scheme $(\mathcal{A}, \mathcal{B})$.

In [1] the primary quantities we presented were the ratios of particular BSM matrix elements over the SM one [4]

$$R_i = \frac{\langle Q_i \rangle}{\langle Q_1 \rangle}.\tag{21}$$

So we now consider the Z factors needed for these ratios. Introducing some notation for the projected vertex functions

$$\Lambda_{ij}^{\mathcal{A}} = P_j^{\mathcal{A}} \left[\Pi_i^{bare} \right] , \quad \mathcal{Z}_{ij}^{(\mathcal{A}, \mathcal{B})} = \frac{Z_{ij}^{(\mathcal{A}, \mathcal{B})}}{Z_{11}^{(\mathcal{A}, \mathcal{B})}} .\tag{22}$$

---

[3] In order to define a massless renormalisation scheme, the renormalisation condition is actually imposed in the chiral limit. However the quark mass dependence of the vertex functions Πs is very mild and the chiral extrapolations are perfectly under control. In order to simplify the discussion, we omit any reference to the finite quark mass effects in this section

[4] In [1] the results are given in the SUSY basis, here we worked in the NPR basis of Eq. 7. In particular O_4 and O_5 in the SUSY basis are now related to Q_2 and Q_3 in the NPR basis. The change of basis is given explicitly in Appendix VII D

From Eq. (20), neglecting the mixing of the $(27, 1)$ with the other operators, one finds that the quantity

$$\mathcal{Z}^{(\mathcal{A},\mathcal{B})}(\mu, a) = \frac{\Lambda_{11}^{\mathcal{A}}(\mu, a)}{F_{11}^{\mathcal{A}}} \times F^{\mathcal{A}} \times \left(\Lambda^{\mathcal{A}}(\mu, a)\right)^{-1}, \tag{23}$$

is independent of $\mathcal{B}$, which is the choice of the projector for the denominator of Eq.(20). Therefore, although in principle we have defined four RI-SMOM schemes $(\gamma_\mu, \gamma_\mu), (\gamma_\mu, \slashed{q}), (\slashed{q}, \gamma_\mu), (\slashed{q}, \slashed{q})$, in this work we mainly consider the "diagonal" schemes, for which $\mathcal{A} = \mathcal{B}$, namely (γ_μ, γ_μ) and $(\slashed{q}, \slashed{q})$.

III. NON-EXCEPTIONAL SCHEMES

A. Choice of projectors

For the quark wave function renormalisation, we make use of two different definitions of Z_q. The factors Z_q/Z_V are determined by imposing the condition

$$\frac{Z_V}{Z_q} P_V [\Pi_V] = F_V . \tag{24}$$

The two projectors we use are $P_V^{(\gamma^\mu)}$ and $P_V^{(\slashed{q})}$, they are defined explicitly by:

$$\begin{aligned}
\frac{Z_q^{(\gamma^\mu)}}{Z_V} &= \frac{1}{F_V^{(\gamma^\mu)}} P_V^{(\gamma^\mu)} [\Pi_V] = \frac{1}{48} \operatorname{Tr} \left[\gamma^\mu \Pi_V^\mu\right] , \\
\frac{Z_q^{(\slashed{q})}}{Z_V} &= \frac{1}{F_V^{(\slashed{q})}} P_V^{(\slashed{q})} [\Pi_V] = \frac{q^\mu}{12q^2} \operatorname{Tr} \left[\slashed{q} \Pi_V^\mu\right] ,
\end{aligned} \tag{25}$$

where Π_V is the amputated Green's functions of the vector and axial-vector current.

The basis of the four-quark operators is given in Eq. (6), our convention is such that that all the operators are "colour-unmixed". The definition of the γ_μ-projectors is straighforward: they are defined with the same spin-colour structure as their respective operators. Explicitly, for the SM operator we have

$$\left[P_1^{(\gamma^\mu)}\right]_{\beta\alpha;\delta\gamma}^{ba;dc} = \left[(\gamma^\mu)_{\beta\alpha}(\gamma^\mu)_{\delta\gamma} + (\gamma^\mu\gamma^5)_{\beta\alpha}(\gamma^\mu\gamma^5)_{\delta\gamma}\right] \delta^{ba}\delta^{dc} . \tag{26}$$

For the $\slashed{q}$ schemes, following [31], we replace the γ_μ matrices by $\slashed{q}/\sqrt{q^2}$, for example

$$\left[P_1^{(\slashed{q})}\right]_{\beta\alpha;\delta\gamma}^{ba;dc} = \frac{1}{q^2} \left[(\slashed{q})_{\beta\alpha}(\slashed{q})_{\delta\gamma} + (\slashed{q}\gamma^5)_{\beta\alpha}(\slashed{q}\gamma^5)_{\delta\gamma}\right] \delta^{ba}\delta^{dc} . \tag{27}$$

Similarly for the $(8,8)$ doublet we have

$$
\begin{aligned}
\left[P_2^{(\gamma^\mu)}\right]_{\beta\alpha;\delta\gamma}^{ba;dc} &= \left[(\gamma^\mu)_{\beta\alpha}(\gamma^\mu)_{\delta\gamma} - (\gamma^\mu\gamma^5)_{\beta\alpha}(\gamma^\mu\gamma^5)_{\delta\gamma}\right]\delta^{ba}\delta^{dc}, \\
\left[P_3^{(\gamma^\mu)}\right]_{\beta\alpha;\delta\gamma}^{ba;dc} &= \left[\delta_{\beta\alpha}\delta_{\delta\gamma} - (\gamma^5)_{\beta\alpha}(\gamma^5)_{\delta\gamma}\right]\delta^{ba}\delta^{dc}.
\end{aligned}
\tag{28}
$$

For the $\not{q}$ projectors, in the case of P_2, we apply the same recipe as the previous operator. For P_3, we take advantage of the Fierz arrangements to "trade" the S and P Dirac matrices for the vector and axial ones. Explicitly we define

$$
\begin{aligned}
\left[P_2^{(\not{q})}\right]_{\beta\alpha;\delta\gamma}^{ba;dc} &= \frac{1}{q^2}\left[(\not{q})_{\beta\alpha}(\not{q})_{\delta\gamma} - (\not{q}\gamma^5)_{\beta\delta}(\not{q}\gamma^5)_{\delta\gamma}\right]\delta^{ba}\delta^{dc}, \\
\left[P_3^{(\not{q})}\right]_{\beta\alpha;\delta\gamma}^{ba;dc} &= \frac{1}{q^2}\left[(\not{q})_{\beta\alpha}(\not{q})_{\delta\gamma} - (\not{q}\gamma^5)_{\beta\delta}(\not{q}\gamma^5)_{\delta\gamma}\right]\delta^{bc}\delta^{da}.
\end{aligned}
\tag{29}
$$

Where the latter is now "colour-mixed" (this set of projector has already been introduced in [25, 26] in the context of $K \to \pi\pi$ decays).

Finally for the $(6,\bar{6})$ operators we define

$$
\begin{aligned}
\left[P_4^{(\gamma^\mu)}\right]_{\beta\alpha;\delta\gamma}^{ba;dc} &= \left[\delta_{\beta\alpha}\delta_{\delta\gamma} + (\gamma^5)_{\beta\alpha}(\gamma^5)_{\delta\gamma}\right]\delta^{ba}\delta^{dc}, \\
\left[P_5^{(\gamma^\mu)}\right]_{\beta\alpha;\delta\gamma}^{ba;dc} &= \left[\frac{1}{2}(\sigma^{\mu\nu})_{\beta\alpha}(\sigma^{\mu\nu})_{\delta\gamma}\right]\delta^{ba}\delta^{dc},
\end{aligned}
\tag{30}
$$

and

$$
\begin{aligned}
\left[P_4^{(\not{q})}\right]_{\beta\alpha;\delta\gamma}^{ba;dc} &= \frac{1}{p_1^2 p_2^2 - (p_1.p_2)^2}\left[(p_1^\mu(\sigma^{\mu\nu}P_L)p_2^\nu)_{\beta\alpha}\,(p_1^\rho(\sigma^{\rho\sigma}P_L)p_2^\sigma)_{\delta\gamma}\right]\delta^{bc}\delta^{da}, \\
\left[P_5^{(\not{q})}\right]_{\beta\alpha;\delta\gamma}^{ba;dc} &= \frac{1}{p_1^2 p_2^2 - (p_1.p_2)^2}\left[(p_1^\mu(\sigma^{\mu\nu}P_L)p_2^\nu)_{\beta\alpha}\,(p_1^\rho(\sigma^{\rho\sigma}P_L)p_2^\sigma)_{\delta\gamma}\right]\delta^{ba}\delta^{dc},
\end{aligned}
\tag{31}
$$

where $P_{R,L} = \frac{1}{2}(1 \pm \gamma_5)$. Imposing Eq. 18 with the projectors given above defines the various schemes $(\mathcal{A},\mathcal{B})$ where $\mathcal{A}$ and $\mathcal{B}$ are either γ_μ or $\not{q}$

B. Tree-level values

For SM operator the tree-level vertex function reads:

$$
\begin{aligned}
\left[\Pi_1^{(0)}\right]_{\alpha\beta;\gamma\delta}^{ab;cd} &= 2\left[(\gamma^\mu)_{\alpha\beta}(\gamma^\mu)_{\gamma\delta} + (\gamma^\mu\gamma_5)_{\alpha\beta}(\gamma^\mu\gamma_5)_{\gamma\delta}\right]\delta^{ab}\delta^{cd} \\
&\quad - 2\left[(\gamma^\mu)_{\alpha\delta}(\gamma^\mu)_{\gamma\beta} + (\gamma^\mu\gamma_5)_{\alpha\delta}(\gamma^\mu\gamma_5)_{\gamma\beta}\right]\delta^{ad}\delta^{cb},
\end{aligned}
\tag{32}
$$

and equivalently for the other Dirac structures. The projectors act on the vertex functions by simply tracing over the Dirac and colour indices, explicitly the tree-level version of Eq. 18 is

$$
P_j\left[\Pi_i^{(0)}\right] = [P_j]_{\beta\alpha;\delta\gamma}^{ba;dc}\left[\Pi_i^{(0)}\right]_{\alpha\beta;\gamma\delta}^{ab;cd} = F_{ij}.
\tag{33}
$$

Volume	a^{-1} [GeV]	am_{ud}^{sea} $(= am_{ud}^{\text{val}})$	m_π [MeV]	am_s^{sea}	am_s^{phys}
$24^3 \times 64 \times 16$	1.785(5)	0.005, 0.01, 0.02	340, 430, (560)	0.04	0.03224(18)
$32^3 \times 64 \times 16$	2.383(9)	0.004, 0.006, 0.008	300, 360, 410	0.03	0.02477(18)

TABLE II. Summary of the lattice ensemble used in this work. Since the renormalisation is performed with momentum sources, only a few configurations are needed (between ten and twenty for each ensemble).

θ	-0.1875	0	0.1875	0.3750	0.5625	0.7500	0.9375	1.1250	1.3125	1.5000
$(ap)^2$	1.1578	1.2337	1.3120	1.3927	1.4759	1.5614	1.6494	1.7397	1.8325	1.9277
$p[GeV]$	1.92	1.98	2.04	2.11	2.17	2.23	2.29	2.35	2.42	2.48
θ	1.6875	1.8750	2.0625	2.2500	2.4375	2.6250	2.8125	3.0000	3.1875	3.3750
$(ap)^2$	2.0252	2.1252	2.2276	2.3325	2.4397	2.5493	2.6614	2.7758	2.8927	3.0120
$p[GeV]$	2.54	2.60	2.66	2.73	2.79	2.85	2.91	2.97	3.04	3.10

TABLE III. List of momenta for the 24^3 lattices. Here we fix the Fourier mode to $n = 3$ and only change the twist angle θ, see Eq.10.

The corresponding tree-level matrices ($N = 3$ is the number of colours) are

$$
F^{(\gamma^\mu)} = \begin{pmatrix}
256N(N+1) & 0 & 0 & 0 & 0 \\
0 & 256N^2 & -128N & 0 & 0 \\
0 & -128N & 64N^2 & 0 & 0 \\
0 & 0 & 0 & 32N(2N-1) & 96N \\
0 & 0 & 0 & 96N & 96N(2N+1)
\end{pmatrix}, \quad (34)
$$

and

$$
F^{(\slashed{q})} = \begin{pmatrix}
64N(N+1) & 0 & 0 & 0 & 0 \\
0 & 64N^2 & 64N & 0 & 0 \\
0 & -32N & -32N^2 & 0 & 0 \\
0 & 0 & 0 & 8N^2 & 8N \\
0 & 0 & 0 & 8N(N+2) & 8N(2N+1)
\end{pmatrix}. \quad (35)
$$

IV.   NUMERICAL RESULTS

A.   Non-perturbative Z factors

The renormalisation is performed on the same ensembles as in [1], the parameters are summarised in Table II. We implement numerically Eq. 20 and obtain the Λ matrices (as defined in

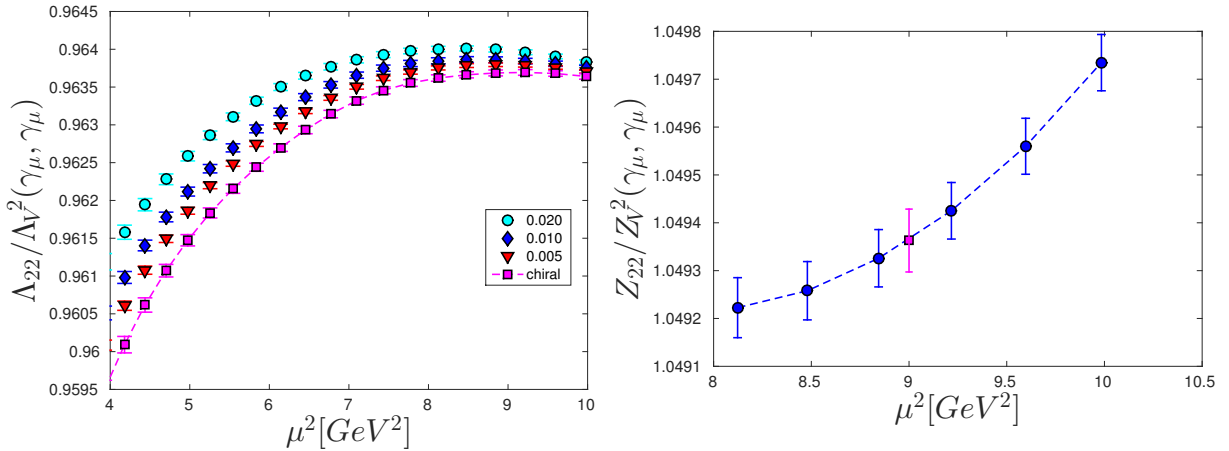| n	3	3	3	3	3	3	3	3	3	3
θ	-0.1	0	0.2	0.4	0.6	0.8	1. 0	1.2	1.4	1.6
$(ap)^2$	0.6710	0.6940	0.7410	0.7896	0.8397	0.8913	0.9446	0.9993	1.0556	1.1134
$p[GeV]$	1.95	1.99	2.05	2.12	2.18	2.25 8	2.32	2.38	2.45	2.51
n	3	4	4	4	4	4	4	4	4	4
θ	1.8	0	0.2	0.4	0.6	0.8	0.9	1. 0	1.1	1.2
$(ap)^2$	1.1728	1.2337	1.2962	1.3602	1.4257	1.4928	1.5269	1.5614	1.5963	1.6316
$p[GeV]$	2.58	2.65	2.71	2.78	2.84	2.92	2.94	2.98	3.01	3.04

TABLE IV. List of momenta for the 32^3 lattices.

FIG. 2. Example of amputated and projected vertex functions at the simulated momenta and quark masses (left) and interpolation of a Z matrix element to the $3\,\mathrm{GeV}$-scale after chiral extrapolation (right). Results are shown for the $\mathrm{SMOM} - (\gamma_\mu, \gamma_\mu)$ scheme on the 24^3 lattice.

Eq 22) at finite quark mass for the the list of momenta listed in Tables III and IV. The parameters for these ensembles are summarised in Table II. We perform a chiral extrapolation, invert the result and then interpolate to the desired scale of 3 GeV. Strictly speaking, there is mismatch from $m_s^{\mathrm{sea}} \neq m_{ud}^{\mathrm{sea}}$, however the quark mass dependence is dominated by the valence sector, the sea contribution plays very little rôle here. Furthermore, for the $\mathrm{RI} - \mathrm{SMOM}$ schemes the light quark mass-dependence is very mild, practically invisible at our renormalisation scale even within our high statistical resolution, and so we consider any associated systematic to be negligible.

Due to the use of partially twisted boundary conditions, we can simulate momenta arbitrarily close to the targeted point, hence only a very small, well controlled, interpolation (performed with a quadratic Ansatz) is required. We illustrate these points in Fig. 2. The numerical results for the Z factors at $3\,\mathrm{GeV}$ are given in tables V,VI, VII, VIII,IX and X.

In principle we only need momenta close to the scale we wish to present our final results at (here $\mu = 3\,\text{GeV}$), however it is useful to compute the Z factors for a larger range, say between 2 and 3 GeV. We can then compare the non-perturbative scale evolution to its perturbative approximation and estimate the effects of truncating the perturbative series for the various schemes. Furthermore, since the running has a continuum limit, we also obtain a nice handle on the discretisation effects.

B. Conversion to $\overline{\text{MS}}$

It is commonplace to convert the renormalised matrix elements computed on the lattice to the $\overline{\text{MS}}$ scheme. In that way, the Wilson coefficients can be combined with the matrix elements to produce phenomenological predictions. The conversion from the $\text{RI} - \text{MOM}$ or $\text{RI} - \text{SMOM}$ to $\overline{\text{MS}}$ is done in continuum perturbation theory. The matching coefficients are known at the one-loop level for $\text{RI} - \text{MOM}$ from [32] and [6]. The situation is different for the $\text{RI} - \text{SMOM}$ schemes: the relevant conversion factors of the $(27, 1)$ operator have been computed in [31]. The conversion matrix for the $(8, 8)$ operators can be extracted from [33] where the conversion was computed for the $\Delta S = 1$ $K \to \pi\pi$ four-quark operators. For the $(6, \bar{6})$ operators, the coefficients were unknown and have been computed for this work. The full expression can be found in Appendix VII B.

To obtain α_s at $\mu = 3$ GeV in the three-flavour theory, we start from $\alpha_s(M_Z) = 0.1185(6)$, we use the four-loop running given in [34, 35] to compute the scale evolution down to the appropriate charm scale, while changing the number of flavours when crossing a threshold, and then run back up to 3 GeV in the three-flavour theory.

The values of the one-loop conversion matrices and the Z factors in $\overline{\text{MS}}$ (ie the Z factors which convert our bare matrix elements to $\overline{\text{MS}}$) are given in tables V,VI, VII, VIII,IX and X. For completeness, we also give the conversion factor for the original $\text{RI} - \text{MOM}$ scheme (the equivalent of the second columns of the above-listed tables)

$$R^{\overline{\text{MS}} \leftarrow \text{RI-MOM}}(3 \text{ GeV}) = \begin{pmatrix} 1.01711 & 0 & 0 & 0 & 0 \\ 0 & 0.97795 & -0.13228 & 0 & 0 \\ 0 & 0.00599 & 1.21233 & 0 & 0 \\ 0 & 0 & 0 & 1.11023 & 0.016719 \\ 0 & 0 & 0 & 0.06318 & 1.052524 \end{pmatrix}. \tag{36}$$

The conversion to $\overline{\text{MS}}$ is then given by $Z^{\overline{\text{MS}}} = R^{\overline{\text{MS}} \leftarrow (\text{scheme})} \times Z^{(\text{scheme})}$ where (scheme) can be $\text{RI} - \text{MOM}$, (γ_μ, γ_μ), $(\slashed{q}, \gamma_\mu)$, $(\gamma_\mu, \slashed{q})$ or $(\slashed{q}, \slashed{q})$.

We observe that in general, the "diagonal" schemes (γ_μ, γ_μ) and $(\not q, \not q)$ have a better perturbative convergence than the off-diagonal ones. At 3 GeV, the conversion matrices are rather close to the identity (which probably explains why our results agree so well with SWME). For our two favorite schemes, we find that after conversion to $\overline{\rm MS}$, the numbers agree rather well. The convergence of the perturbative series and the effects of the lattice artefacts could also be estimated by looking at the step-scaling matrices, which we do in the next section (see also Appendix VII C).

C. Non-perturbative scale evolution and comparison with perturbation theory

The scale evolution matrix, $\sigma(\mu_1, \mu_2)$ is a rich source of information, in particular it helps us to estimate the systematic errors affecting the renormalisation procedure. We define

$$\sigma(\mu_1, \mu_2, a) = Z(\mu_1, a) Z^{-1}(\mu_2, a) , \tag{37}$$

where Z is the 5×5 matrix defined in Eq. 20. (Although in practice we take the chiral limit of the right hand side of Eq. 37, once again in order to simplify the notation, we discard any reference to the quark masses.)

The scale evolution matrix has a universal continuum limit and may be directly compared to continuum perturbation theory. The continuum extrapolation

$$\sigma(\mu_1, \mu_2) = \lim_{a^2 \to 0} \sigma(\mu_1, \mu_2, a) . \tag{38}$$

is performed assuming a linear behaviour in a^2. For this step the use of twisted boundary conditions is essential, since it allows us to vary μ continuously holding the momentum orientation (and $\mathcal{O}(a^2)$ coefficients) fixed.

The continuum extrapolation of $\sigma_{ii}(2\,{\rm GeV}, \mu)$, where $2\,{\rm GeV} \leq \mu \leq 3\,{\rm GeV}$, is shown in Figs. 7-9, compared with continuum perturbation theory. We find in general good agreement with the perturbative series, indicating that the a^2 extrapolation is valid and discretisation effects are under control. An example of off-diagonal matrix elements can be found in Fig 10.

By comparing the non-perturbative running to its perturbative approximation, we can estimate the quality of the perturbative series for the various schemes. This is important in view of the perturbative macthing of the NPR factors to $\overline{\rm MS}$. In order to compare the scale evolution matrix to the perturbative estimates, it is useful to construct the quantity $\sigma(\mu_1, \mu_2)\sigma_{\rm PT}^{-1}(\mu_1, \mu_2)$, which is equal to $1_{5\times5}$ up to higher-order terms not included in the perturbative expansions, residual discretisation effects, and non-perturbative contributions. These quantities are shown in Figs. 11-

$Z^{\overline{\text{MS}}}$	$R^{\overline{\text{MS}}\leftarrow\text{RI–SMOM}}$	$Z^{\text{RI–SMOM}}$	scheme
0.92022(26)	1.00414	0.91642(26)	(γ_μ, γ_μ)
0.97675(48)	0.95205	1.02593(51)	$(\gamma_\mu, \slashed{q})$
0.89123(23)	1.04320	0.85432(22)	$(\slashed{q}, \gamma_\mu)$
0.94796(34)	0.99112	0.95645(34)	$(\slashed{q}, \slashed{q})$

TABLE V. Z/Z_V^2 factors for the $(27,1)$ operators at $3\,\text{GeV}$ for $a = a_{\mathbf{24}}$.

$Z^{\overline{\text{MS}}}$	$R^{\overline{\text{MS}}\leftarrow\text{RI–SMOM}}$	$Z^{\text{RI–SMOM}}$	scheme
$\begin{pmatrix} 1.05043(7) & 0.28197(37) \\ 0.05654(23) & 0.95348(189) \end{pmatrix}$	$\begin{pmatrix} 1.00084 & 0.00506 \\ 0.01576 & 1.08781 \end{pmatrix}$	$\begin{pmatrix} 1.04936(7) & 0.27732(38) \\ 0.03677(21) & 0.87249(174) \end{pmatrix}$	(γ_μ, γ_μ)
$\begin{pmatrix} 1.11482(33) & 0.29951(46) \\ 0.06115(24) & 1.01655(183) \end{pmatrix}$	$\begin{pmatrix} 0.94876 & 0.00506 \\ 0.01576 & 1.03572 \end{pmatrix}$	$\begin{pmatrix} 1.17481(35) & 0.31048(50) \\ 0.04117(23) & 0.97677(178) \end{pmatrix}$	$(\gamma_\mu, \slashed{q})$
$\begin{pmatrix} 0.98777(27) & 0.26988(33) \\ 0.06483(20) & 0.95664(185) \end{pmatrix}$	$\begin{pmatrix} 1.05293 & 0.00506 \\ 0.00599 & 1.08130 \end{pmatrix}$	$\begin{pmatrix} 0.93785(26) & 0.25207(32) \\ 0.05475(18) & 0.88332(171) \end{pmatrix}$	$(\slashed{q}, \gamma_\mu)$
$\begin{pmatrix} 1.05116(7) & 0.28745(40) \\ 0.06938(21) & 1.01946(179) \end{pmatrix}$	$\begin{pmatrix} 1.00084 & 0.00506 \\ 0.00599 & 1.02921 \end{pmatrix}$	$\begin{pmatrix} 1.04996(7) & 0.28221(41) \\ 0.06129(20) & 0.98888(174) \end{pmatrix}$	$(\slashed{q}, \slashed{q})$

TABLE VI. Z/Z_V^2 matrices for the $(8,8)$ operators at $\mu = 3\,\text{GeV}$ for $a = a_{\mathbf{24}}$.

$Z^{\overline{\text{MS}}}$	$R^{\overline{\text{MS}}\leftarrow\text{RI–SMOM}}$	$Z^{\text{RI–SMOM}}$	scheme
$\begin{pmatrix} 0.93350(166) & -0.02688(26) \\ -0.33065(42) & 1.16123(94) \end{pmatrix}$	$\begin{pmatrix} 1.02004 & 0.00968 \\ -0.05621 & 1.11206 \end{pmatrix}$	$\begin{pmatrix} 0.91754(162) & -0.03625(25) \\ -0.25096(45) & 1.04239(86) \end{pmatrix}$	(γ_μ, γ_μ)
$\begin{pmatrix} 0.99155(159) & -0.02798(27) \\ -0.35554(54) & 1.23927(126) \end{pmatrix}$	$\begin{pmatrix} 0.96796 & 0.00968 \\ -0.05621 & 1.05997 \end{pmatrix}$	$\begin{pmatrix} 1.02719(164) & -0.04058(27) \\ -0.28096(58) & 1.16700(121) \end{pmatrix}$	$(\gamma_\mu, \slashed{q})$
$\begin{pmatrix} 0.92457(145) & -0.02343(19) \\ -0.41226(142) & 1.19248(49) \end{pmatrix}$	$\begin{pmatrix} 1.01556 & 0.01118 \\ -0.07860 & 1.11952 \end{pmatrix}$	$\begin{pmatrix} 0.91375(143) & -0.03477(18) \\ -0.30410(119) & 1.06273(45) \end{pmatrix}$	$(\slashed{q}, \gamma_\mu)$
$\begin{pmatrix} 0.98180(136) & -0.02422(20) \\ -0.44382(148) & 1.27309(83) \end{pmatrix}$	$\begin{pmatrix} 0.96348 & 0.01118 \\ -0.07860 & 1.06744 \end{pmatrix}$	$\begin{pmatrix} 1.02296(142) & -0.03894(20) \\ -0.34046(131) & 1.18980(79) \end{pmatrix}$	$(\slashed{q}, \slashed{q})$

TABLE VII. Z/Z_V^2 matrices for the $(6,\bar{6})$ operators at $\mu = 3\,\text{GeV}$ for $a = a_{\mathbf{24}}$.

14. When running from 3 to 2 GeV, we find that these effects are typically of order a few percents, and in many instances much less.

$Z^{\overline{\mathrm{MS}}}$	$R^{\overline{\mathrm{MS}}\leftarrow\mathrm{RI-SMOM}}$	$Z^{\mathrm{RI-SMOM}}$	scheme
0.94526(26)	1.00414	0.94137(26)	(γ_μ, γ_μ)
0.99554(67)	0.95205	1.04568(70)	$(\gamma_\mu, \slashed{q})$
0.91915(53)	1.04320	0.88109(51)	$(\slashed{q}, \gamma_\mu)$
0.96999(32)	0.99112	0.97868(32)	$(\slashed{q}, \slashed{q})$

TABLE VIII. Z/Z_V^2 factors for the $(27,1)$ operators at $3\,\mathrm{GeV}$ for $a = a_{\mathbf{32}}$.

$Z^{\overline{\mathrm{MS}}}$	$R^{\overline{\mathrm{MS}}\leftarrow\mathrm{RI-SMOM}}$	$Z^{\mathrm{RI-SMOM}}$	scheme
$\begin{pmatrix} 1.04740(14) & 0.27818(76) \\ 0.04391(15) & 0.87386(157) \end{pmatrix}$	$\begin{pmatrix} 1.00084 & 0.00506 \\ 0.01576 & 1.08781 \end{pmatrix}$	$\begin{pmatrix} 1.04639(14) & 0.27391(76) \\ 0.02521(13) & 0.79935(145) \end{pmatrix}$	(γ_μ, γ_μ)
$\begin{pmatrix} 1.10288(81) & 0.29313(92) \\ 0.04731(16) & 0.92432(154) \end{pmatrix}$	$\begin{pmatrix} 0.94876 & 0.00506 \\ 0.01576 & 1.03572 \end{pmatrix}$	$\begin{pmatrix} 1.16230(85) & 0.30423(97) \\ 0.02799(15) & 0.88781(149) \end{pmatrix}$	$(\gamma_\mu, \slashed{q})$
$\begin{pmatrix} 0.99359(64) & 0.26772(73) \\ 0.05169(22) & 0.87793(156) \end{pmatrix}$	$\begin{pmatrix} 1.05293 & 0.00506 \\ 0.00599 & 1.08130 \end{pmatrix}$	$\begin{pmatrix} 0.94344(61) & 0.25037(70) \\ 0.04258(20) & 0.81054(144) \end{pmatrix}$	$(\slashed{q}, \gamma_\mu)$
$\begin{pmatrix} 1.04908(16) & 0.28286(83) \\ 0.05496(25) & 0.92821(156) \end{pmatrix}$	$\begin{pmatrix} 1.00084 & 0.00506 \\ 0.00599 & 1.02921 \end{pmatrix}$	$\begin{pmatrix} 1.04795(16) & 0.27806(84) \\ 0.04730(24) & 0.90024(152) \end{pmatrix}$	$(\slashed{q}, \slashed{q})$

TABLE IX. Z/Z_V^2 matrices for the $(8,8)$ operators at $\mu = 3\,\mathrm{GeV}$ for $a = a_{\mathbf{32}}$.

$Z^{\overline{\mathrm{MS}}}$	$R^{\overline{\mathrm{MS}}\leftarrow\mathrm{RI-SMOM}}$	$Z^{\mathrm{RI-SMOM}}$	scheme
$\begin{pmatrix} 0.86595(130) & -0.01245(18) \\ -0.32627(79) & 1.21084(92) \end{pmatrix}$	$\begin{pmatrix} 1.02004 & 0.00968 \\ -0.05621 & 1.11206 \end{pmatrix}$	$\begin{pmatrix} 0.85132(127) & -0.02253(17) \\ -0.25036(76) & 1.08769(83) \end{pmatrix}$	(γ_μ, γ_μ)
$\begin{pmatrix} 0.91256(128) & -0.01252(19) \\ -0.34790(98) & 1.28201(145) \end{pmatrix}$	$\begin{pmatrix} 0.96796 & 0.00968 \\ -0.05621 & 1.05997 \end{pmatrix}$	$\begin{pmatrix} 0.94555(132) & -0.02502(19) \\ -0.27808(96) & 1.20814(137) \end{pmatrix}$	$(\gamma_\mu, \slashed{q})$
$\begin{pmatrix} 0.86318(125) & -0.01153(18) \\ -0.34762(135) & 1.21953(90) \end{pmatrix}$	$\begin{pmatrix} 1.05293 & 0.00506 \\ 0.00599 & 1.08130 \end{pmatrix}$	$\begin{pmatrix} 0.85271(123) & -0.02332(17) \\ -0.25065(122) & +1.08770(81) \end{pmatrix}$	$(\slashed{q}, \gamma_\mu)$
$\begin{pmatrix} 0.90945(122) & -0.01146(19) \\ -0.37164(161) & 1.29174(159) \end{pmatrix}$	$\begin{pmatrix} 0.96348 & 0.01118 \\ -0.07860 & 1.06744 \end{pmatrix}$	$\begin{pmatrix} 0.94715(127) & -0.02590(19) \\ -0.27842(149) & 1.20822(149) \end{pmatrix}$	$(\slashed{q}, \slashed{q})$

TABLE X. Z/Z_V^2 matrices for the $(6,\bar{6})$ operators at $\mu = 3\,\mathrm{GeV}$ for $a = a_{\mathbf{32}}$.

$\sigma(2\text{GeV}, 3\text{GeV})^{\overline{\text{MS}}}$	$\sigma(2\text{GeV}, 3\text{GeV})^{\text{RI}-\text{SMOM}}$	scheme
1.0194(9)	1.0186(9)	(γ_μ, γ_μ)
1.0649(32)	1.0761(32)	$(\gamma_\mu, \slashed{q})$
0.9963(26)	0.9879(25)	$(\slashed{q}, \gamma_\mu)$
1.0428(12)	1.0448(12)	$(\slashed{q}, \slashed{q})$

TABLE XI. Continuum running factor between 3 and 2 GeV for the $(27, 1)$ operator and the various intermediate schemes. In the first column we give the results converted to $\overline{\text{MS}}$, whereas in the middle column the results are in the RI-SMOM scheme and are purely non-perturbative.

$\sigma(2\text{GeV}, 3\text{GeV})^{\overline{\text{MS}}}$	$\sigma(2\text{GeV}, 3\text{GeV})^{\text{RI}-\text{SMOM}}$	scheme
$\begin{pmatrix} 1.0177(11) & 0.1453(22) \\ 0.0095(7) & 0.7873(44) \end{pmatrix}$	$\begin{pmatrix} 1.0198(11) & 0.1583(24) \\ 0.0023(6) & 0.7718(44) \end{pmatrix}$	(γ_μ, γ_μ)
$\begin{pmatrix} 1.0634(37) & 0.1506(22) \\ 0.0105(7) & 0.8256(65) \end{pmatrix}$	$\begin{pmatrix} 1.0778(37) & 0.1667(22) \\ 0.0024(7) & 0.8168(65) \end{pmatrix}$	$(\gamma_\mu, \slashed{q})$
$\begin{pmatrix} 0.9743(35) & 0.1347(29) \\ 0.0134(18) & 0.7863(49) \end{pmatrix}$	$\begin{pmatrix} 0.9650(34) & 0.1371(29) \\ 0.0108(17) & 0.7735(49) \end{pmatrix}$	$(\slashed{q}, \gamma_\mu)$
$\begin{pmatrix} 1.0199(10) & 0.1397(28) \\ 0.0142(18) & 0.8241(74) \end{pmatrix}$	$\begin{pmatrix} 1.0205(10) & 0.1438(30) \\ 0.0114(18) & 0.8184(73) \end{pmatrix}$	$(\slashed{q}, \slashed{q})$

TABLE XII. Same for the running matrix of the $(8, 8)$ operators.

$\sigma(2\text{GeV}, 3\text{GeV})^{\overline{\text{MS}}}$	$\sigma(2\text{GeV}, 3\text{GeV})^{\text{RI}-\text{SMOM}}$	scheme
$\begin{pmatrix} 0.8402(36) & 0.0068(5) \\ -0.1356(18) & 1.1446(16) \end{pmatrix}$	$\begin{pmatrix} 0.8379(35) & 0.0025(6) \\ -0.1285(18) & 1.1203(16) \end{pmatrix}$	(γ_μ, γ_μ)
$\begin{pmatrix} 0.8795(58) & 0.0075(5) \\ -0.1426(21) & 1.1968(38) \end{pmatrix}$	$\begin{pmatrix} 0.8868(59) & 0.0028(6) \\ -0.1354(20) & 1.1819(37) \end{pmatrix}$	$(\gamma_\mu, \slashed{q})$
$\begin{pmatrix} 0.8288(62) & 0.0084(19) \\ -0.1795(76) & 1.1602(26) \end{pmatrix}$	$\begin{pmatrix} 0.8278(63) & 0.0033(20) \\ -0.1705(72) & 1.1337(25) \end{pmatrix}$	$(\slashed{q}, \gamma_\mu)$
$\begin{pmatrix} 0.8612(60) & 0.0092(19) \\ -0.1853(84) & 1.2155(60) \end{pmatrix}$	$\begin{pmatrix} 0.8697(61) & 0.0034(21) \\ -0.1772(80) & 1.1982(59) \end{pmatrix}$	$(\slashed{q}, \slashed{q})$

TABLE XIII. Same for the running matrix of the $(6, \bar{6})$ operators.

V.   RI-MOM RENORMALISATION SCHEME

In addition to the RI-SMOM renormalisation schemes used to obtain our main results [1], we also implemented RI-MOM renormalisation conditions for the intermediate scheme. The RI-MOM scheme differs in the kinematic configuration of the vertex functions, which depend on a single momentum vector (obtained by setting $p_1 = p_2$ in Eq. (13)). Vertex functions in this "exceptional" configuration can have large contributions from infrared poles which go as inverse powers of the quark mass (m_π^2) and momenta; as our renormalisation matrices are defined in the chiral limit $m \to 0$ (here and throughout this section $m = m_{\text{bare}} + m_{\text{res}}$) we have an unphysical divergence due to this scheme, which must be subtracted. These pole contributions are suppressed by powers of p^2 but in practice turn out to be large for momenta accessible in our Rome Southampton window.

As the $m \to 0$ limit is approached the raw RI-MOM data clearly suffers from pole contamination, the effect of these pion poles is clearly visible in our data, in particular in the Λ_{i3} and Λ_{i4} elements (Fig. 3); in contrast the RI-SMOM data have only a weak mass dependence and tend to Z^{-1} in the $m \to 0$ limit (Fig 4).

At large $\mu = \sqrt{p^2}$ the matrix of vertex functions Λ will become block diagonal in the chiral limit if the effects of spontaneous chiral symmetry breaking are suppressed. In the RI-MOM scheme chiral symmetry breaking effects can be extremely enhanced in the $m \to 0$ limit; as a result the chiral structure is strongly broken. This can be seen for example in Fig. 5 (right).

We focus first on the chiral extrapolation and work at fixed momentum. In order to extract Z_{ij} from the RI-MOM data, we fit the mass dependence of the vertex functions Λ_{ij}. In principle we expect the vertex function to exhibit poles which go like $1/m$ and $1/m^2$ (see for example [17]), and so will be described by the general form

$$\Lambda_{ij}(a, \mu, m) = Z_{ij}^{-1}(a, \mu) + \frac{B_{ij}(a, \mu)}{(am)} + \frac{C_{ij}(a, \mu)}{(am)^2} + D_{ij}(a, \mu)(am) + \mathcal{O}((am)^2). \qquad (39)$$

First, we observe that not all the matrix elements require a pole subtraction. In that case, we just perform a linear fit in the quark mass (ie $B = C = 0$) with the three (lightest) unitary [5]. quark masses: $am_{\text{bare}} = 0.005, 0.01, 0.02$ on the 24^3 and $0.004, 0.006, 0.008$ on the 32^3. The chirally-allowed elements which suffer from those pole contaminations are $\Lambda_{23}, \Lambda_{33}, \Lambda_{44}$ and Λ_{55} and the chirally-forbidden are $\Lambda_{24}, \Lambda_{34}, \Lambda_{44}$ and Λ_{53}. In this case, our main results are obtained on the same data with a single pole fit Ansatz $C = D = 0$.

---

[5] Strictly speaking the setup is unitary in the light quark sector $m_{\text{light}}^{\text{val}} = m_{\text{light}}^{\text{sea}}$, but partially quenched for the strange as $m_{\text{s}}^{val} = m_{\text{light}}^{\text{val}} \neq m_{\text{s}}^{\text{sea}}$, however we have checked this effect is negligible within our systematic errors

More explicitly, we used a 'linear fit' method [16, 24] to remove the $1/m$ contributions to the RI-MOM vertex functions. Here we multiply the data by am and fit $am\Lambda_{ij} = (am)Z_{ij}^{-1} + B_{ij} + \mathcal{O}((am)^2)$ to a straight line to determine Z_{ij}^{-1}. This gives results equivalent to fitting Λ to the form $A + B/m$. We observed that $am\Lambda$ is consistent with linear am behavior to justify neglecting the $(am)^2$ term, and also found the data after subtracting the pole contribution is linear. After subtracting the pole we find good restoration of the chiral block structure for the 32^3 ensemble (Table XV), The chiral restoration is not as good on the 24^3 ensemble, the residual matrix elements are of the order of a few %. However we observed that they do affect the physical matrix elements, and that different fit procedure give the same residual, see below and Table XIV.

Since this infrared contamination completely dominates some of the raw data in the RI-MOM scheme, we investigated the effect of this pole subtraction, in particular we want to have a reasonable estimate of the systematic error associated with the procedure. On the 24^3, we used another ensemble $m_{\text{light}}^{\text{val}} = m_{\text{light}}^{\text{sea}} = 0.03$ and have implemented different fit forms. We fit each of the Λ_{ij} with the forms $A + Dm$ (**fit-0**), $A + B/m + Dm$ (**fit-1**), and $A + C/m^2 + Dm$ (**fit-2**). We find that in cases with significant singular behavior, the **fit-1** has $\chi^2 < 1$ and **fit-2** has $\chi^2 \gg 1$. For $j = 1, 2, 5$ there is no evidence of $1/m$ behavior and the results are compatible with **fit-0**. The fits are shown in Fig. 3 for the chirally allowed elements Λ_{23}, Λ_{33}, Λ_{44}, and Λ_{54}. From this we conclude that any $1/m^2$ dependence is to a large degree suppressed in the range of m_{val} for which we have data, and we determine Z_{ij}^{-1} assuming the form of **fit-1**.

As a check on the procedure we compare the **fit-1** results on the 24^3 ensemble to the linear fit procedure. For the linear fit method we threw out the heaviest ($am = 0.03$) mass point because we found a degradation in the χ^2 (though central values remain consistent), and which we attribute to neglecting the quadratic term. The results from the two subtraction methods are shown in Fig. 3 and Table XIV. There is a slight tension in the extrapolated results which highlights that some uncontrolled systematic due to specifics of the subtraction procedure may remain.

We also implemented Bayesian fits using the `lsqfit` package [6] to include additional terms from Eq. (39) without requiring the number of data points to exceed the number of fit parameters. Table XIV compares results of frequentist and Bayesian fitting on the 24^3 ensemble, for both chirally allowed and forbidden elements. The Bayesian fit of the full form (39) is consistent with the results of the other methods but with larger uncertainties. For the chirally-forbidden elements, the single pole fits (**fit-1** and Lin. fit) find values which differ significantly from zero, whereas the Bayesian method finds best-fit values very close to zero, but with errors comparable to the size of

---

[6] https://github.com/gplepage/lsqfit
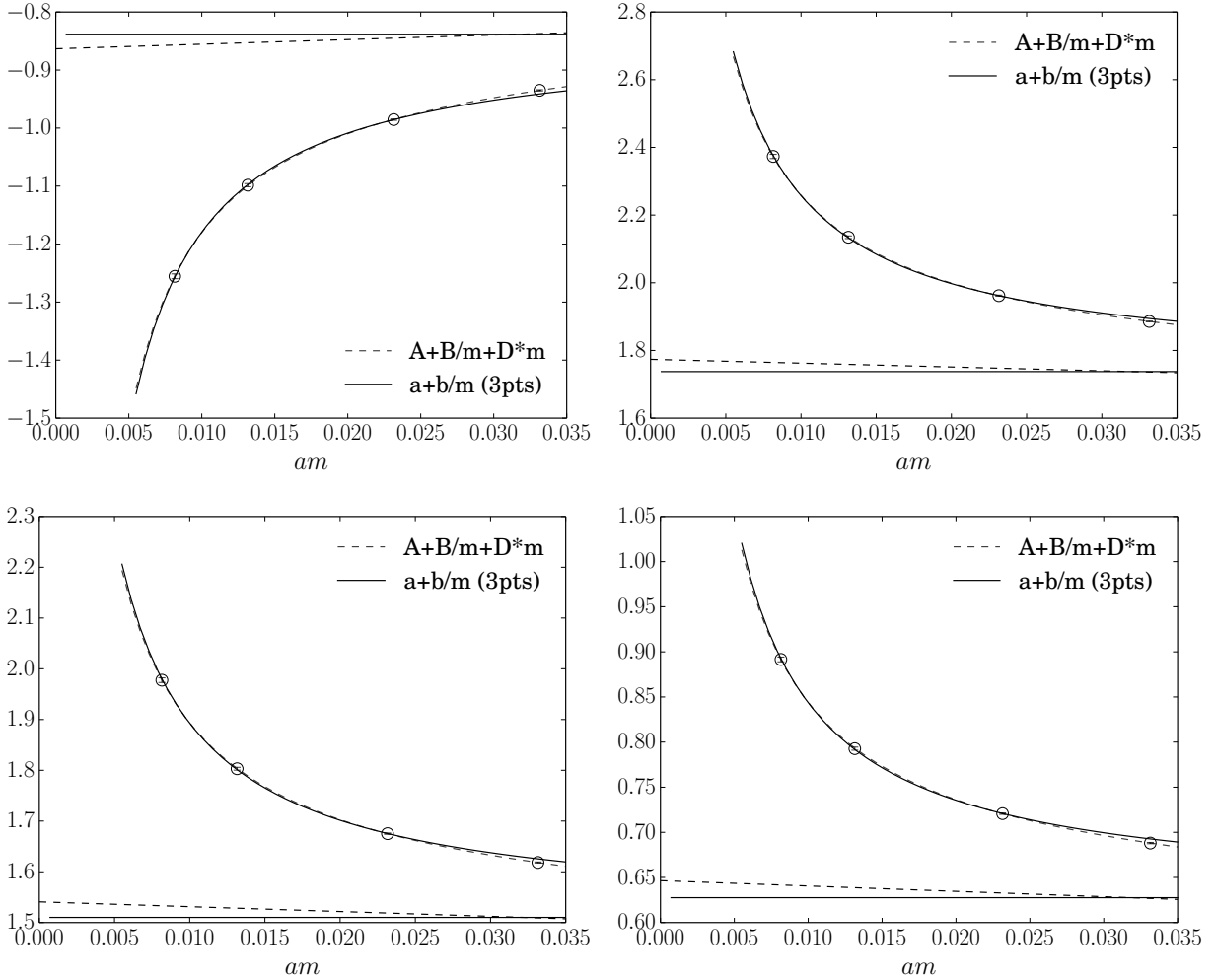
the central values in the single pole case.

FIG. 3. Chirally-allowed RI-MOM vertex functions with singular behaviour from the 24^3 ensemble. The result of fitting the raw data (circles) to **fit-1** (dotted line) and a fit to the lightest three points with the form $a + b/m$ (solid line), along with the result of subtracting the single pole contribution from each of the fits (same line type as respective fits through data). Quantities shown from left to right are $\Lambda_{23}, \Lambda_{33}$ (first row) and $\Lambda_{44}, \Lambda_{54}$ (second row) at fixed momentum close to 3 GeV.

As another consistency check of the method, we should also find an approximate recovery of the block diagonal structure expected from chiral symmetry after removing the singular parts of the data. Although to a decent approximation the terms that are chirally-forbidden are suppressed after the pole subtraction, we find that the values are statistically non-zero and the magnitude of chirally-forbidden elements tend to be larger for the pole-subtracted ($\Lambda_{i,3/4}$) compared to elements that do not require pole subtraction ($\Lambda_{i,1/2/4}$). Fig. 5 shows the mass and μ dependence of chirally-forbidden RI-MOM vertex functions for a case without discernible singular structure (Λ_{12}, left),
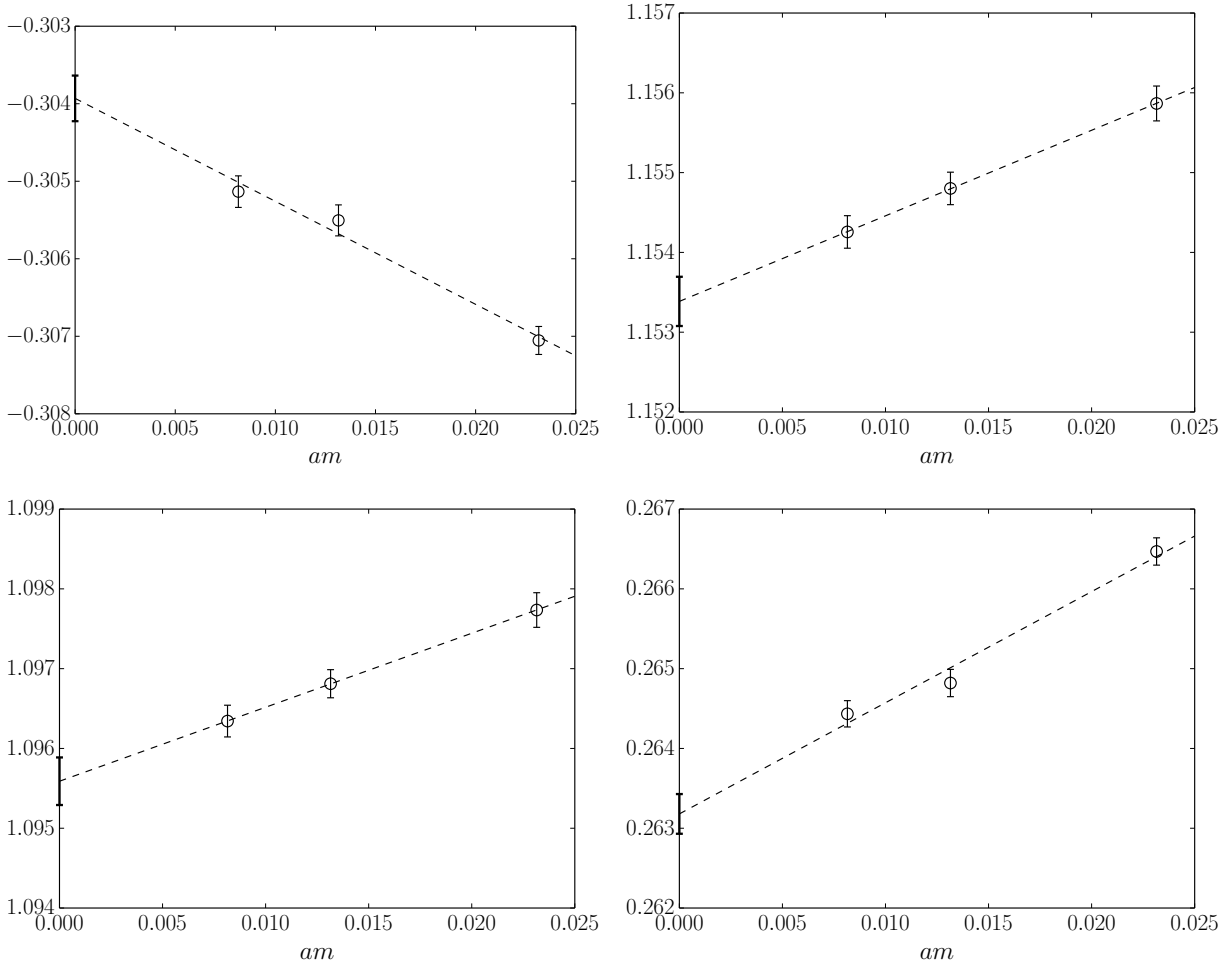
FIG. 4. Same as Fig. 3, from left to right: $\Lambda_{23}, \Lambda_{33}$ (first row) and $\Lambda_{44}, \Lambda_{54}$ (second row), for the non-exceptional (γ_μ, γ_μ) scheme. Here we fix the momentum μ close to 3 GeV.. In that case we observed a very mild, linear, quark mass dependence. In contrast to the RI-MOM case, no pole subtraction is required (we show the vertex function without applying any pole strubaction procedure).

and where the pole behavior is clearly visible (Λ_{24}, right). These results should be contrasted with the RI-SMOM results shown in Fig. 6, where in all cases the chirally-forbidden elements extrapolate very nearly to zero.

On the 32^3 ensemble we also compare results of including the single pole or both poles using a Bayesian fit, and results from the linear fit method, shown in Table XV. The results again agree with the linear fit results but have larger associated uncertainties. Note here the chirally-forbidden elements obtained from the linear fit method are much smaller than in the 24^3 case and are in fact zero within errors. We also tried including the $1/m$ terms in 'global' fits by constraining the $1/m$ coefficient coefficient in Λ_{i3} to be the negative of the coefficient in Λ_{i4}, which we observed to be the case. Althought this strategy seems to improve somewhat the fit quality, the numerical resuls

$Z_V^2 Z_{ij}^{-1}$	Lin. Fit meth.	Freq. $\frac{1}{m}$	Bayes* $\frac{1}{m}$	Bayes $\frac{1}{m}, \frac{1}{m^2}$
23	-0.835(3)	-0.863(10)	-0.849(28)	-0.880(41)
33	1.733(4)	1.774(14)	1.758(40)	1.791(58)
44	1.506(3)	1.541(11)	1.535(29)	1.548(42)
54	0.625(2)	0.646(7)	0.639(18)	0.657(26)
24	0.052(5)	0.063(16)	0.100(45)	0.011(65)
34	-0.077(7)	-0.091(24)	-0.143(68)	0.006(98)
43	-0.065(5)	-0.080(19)	-0.127(51)	0.003(74)
53	-0.038(3)	-0.047(11)	-0.076(29)	-0.001(43)

TABLE XIV. Comparison of fit results on 24^3 using "linear fit method", frequentist fit with $1/m$ term ($1/m^2$ term set to zero), Bayesian fit with only $1/m$ term (* result uses only lightest three masses), and Bayesian fit with both $1/m$ and $1/m^2$ terms. The lower set of values corresponds to chirally-forbidden elements.
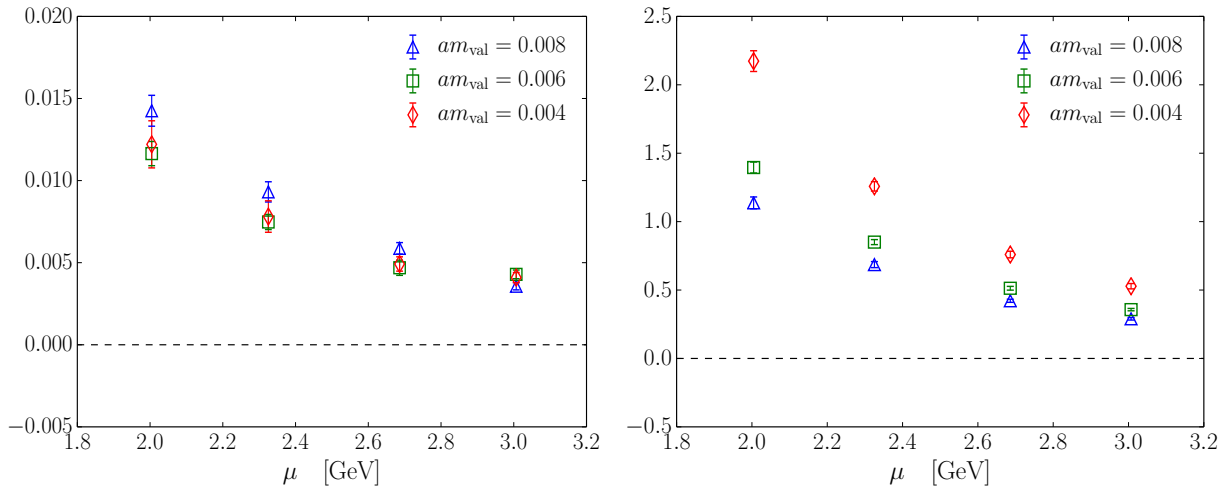
FIG. 5. Left: Example of an amputated and projected Green function in the exceptional RI-MOM scheme at finite quark mass (on 32^3 ensemble) for different momenta. This specific quantity should vanish if chiral symmetry is exact. Right: Example of a RI-MOM vertex function with strong singular behavior. This specific quantity should also vanish if chiral symmetry is exact but is affected by large infrared contaminations.

were essentially unchanged.

We choose two options when we compute our renormalisation matrices: firstly we invert the whole matrix of fit parameters for all Λ_{ij} and secondly we invert only the block diagonal elements of the matrix, zeroing by hand the chirally-forbidden elements. We will label these as the Not Block-Diagonal (NBD) and the Block Diagonal (BD).

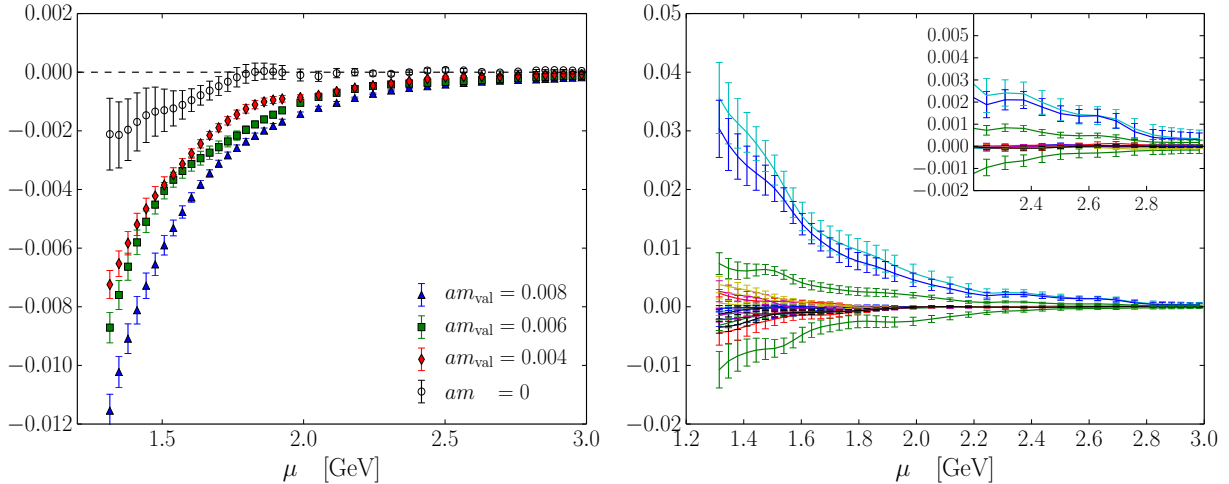Here we list the results for Z-matrices obtained in RI-MOM from the linear fit method. On the

FIG. 6. Left: Example of RI-SMOM (γ_μ, γ_μ) Z-factor at finite quark mass and in the chiral limit (on 32^3 ensemble) for various momenta. Right: Chirally-forbidden renormalisation factors in the (γ_μ, γ_μ) scheme after chiral extrapolation for various momenta.

$Z_V^2 Z_{ij}^{-1}$	Lin. Fit meth.	Bayes $\frac{1}{m}$
23	-0.778(21)	-0.691(107)
33	1.769(31)	1.701(121)
44	1.538(21)	1.461(107)
54	0.570(12)	0.511(81)
24	0.006(34)	-0.036(124)
34	-0.007(53)	0.046(135)
43	-0.018(38)	0.048(127)
53	-0.011(21)	0.072(107)

TABLE XV. Comparison of fit results on 32^3 using "linear fit method", and Bayesian fit including $1/m$ term. The lower set of values corresponds to chirally-forbidden elements at $\mu = 3.01$ GeV.

24^3 ensemble at a fixed value of μ close to 3 GeV ,

$$\frac{Z^{BD}}{Z_V^2} = \begin{pmatrix} 0.88768(13) & 0 & 0 & 0 & 0 \\ 0 & 1.10238(24) & 0.5318(22) & 0 & 0 \\ 0 & 0.04812(16) & 0.5988(14) & 0 & 0 \\ 0 & 0 & 0 & 0.6807(13) & -0.04444(14) \\ 0 & 0 & 0 & -0.4940(18) & 1.18877(50) \end{pmatrix} ,$$

$$\frac{Z^{NBD}}{Z_V^2} = \begin{pmatrix} 0.88771(13) & -0.00732(27) & -0.00305(14) & 0.000479(29) & 0.000017(7) \\ -0.00524(20) & 1.10240(24) & 0.5313(22) & -0.0112(44) & 0.00068(31) \\ 0.000335(24) & 0.04817(16) & 0.5999(14) & 0.0297(29) & -0.00125(20) \\ 0.000055(7) & 0.00135(18) & 0.0254(22) & 0.6820(13) & -0.04449(14) \\ 0.000077(9) & 0.00047(23) & 0.0080(26) & -0.4936(18) & 1.18875(50) \end{pmatrix} .$$

$$(40)$$

And the 32^3 at $\mu = 3.01$ GeV,

$$\frac{Z^{BD}}{Z_V^2} = \begin{pmatrix} 0.92128(28) & 0 & 0 & 0 & 0 \\ 0 & 1.0887(10) & 0.480(14) & 0 & 0 \\ 0 & 0.03506(56) & 0.5787(85) & 0 & 0 \\ 0 & 0 & 0 & 0.6592(76) & -0.02996(47) \\ 0 & 0 & 0 & -0.448(10) & 1.2072(12) \end{pmatrix} ,$$

$$\frac{Z^{NBD}}{Z_V^2} = \begin{pmatrix} 0.92129(28) & -0.00310(61) & -0.00101(29) & 0.000219(75) & 0.000000(27) \\ -0.00251(47) & 1.0886(10) & 0.480(14) & -0.004(27) & 0.0001(13) \\ 0.000249(72) & 0.03507(57) & 0.5789(85) & 0.008(17) & 0.00032(82) \\ 0.000021(47) & 0.00038(82) & 0.010(12) & 0.6593(76) & -0.02996(47) \\ 0.000033(53) & 0.00006(96) & 0.004(15) & -0.448(10) & 1.2072(12) \end{pmatrix} .$$

$$(41)$$

It is evident that the BD and NBD Z-matrices are not too dissimilar, we take the difference in results of the operators renormalised using either of these as a systematic for our final RI-MOM results. Our results in the RI-MOM scheme after chiral extrapolation and interpolation to $\mu = 3$ GeV read

$$\frac{Z^{\text{RI-MOM}}}{Z_V^2}(a_{\mathbf{24}}) = \begin{pmatrix} 0.88989(134) & 0 & 0 & 0 & 0 \\ 0 & 1.1015(6) & 0.5299(14) & 0 & 0 \\ 0 & 0.0470(8) & 0.5931(49) & 0 & 0 \\ 0 & 0 & 0 & 0.6744(50) & -0.0429(10) \\ 0 & 0 & 0 & -0.4929(9) & 1.1918(24) \end{pmatrix} , \qquad (42)$$

$$\frac{Z^{\text{RI-MOM}}}{Z_V^2}(a_{\mathbf{32}}) = \begin{pmatrix} 0.9213(11) & 0 & 0 & 0 & 0 \\ 0 & 1.08879(64) & 0.4792(47) & 0 & 0 & 0 \\ 0 & 0.03512(70) & 0.580(11) & 0 & 0 & 0 \\ 0 & 0 & 0 & 0.6602(101) & -0.0301(8) \\ 0 & 0 & 0 & -0.4476(43) & 1.2080(51) \end{pmatrix}. \quad (43)$$

In conclusion, the infrared contamination in some of the RI-MOM vertex functions makes it difficult to extract the Z-factors precisely in the $m \to 0$ limit, where these contributions diverge. These effects also strongly break the chiral structure one expects to recover for $\mu \gg \Lambda_{\text{QCD}}$, though this structure is restored (albeit imperfectly) after subtraction of the pole contributions. For these reasons, we find that the RI-MOM scheme (with exceptional kinematics) suffer from systematic errors which are difficult estimate. Applying different strategies to subtract the poles, we find that final results vary by 5% in the worse case.

In contrast the SMOM procedure strongly suppresses these infrared effects – evidence of chiral symmetry breaking disappears in the $am \to 0$ limit at sufficiently large μ (Fig. 6), and the chirally-allowed Z-factors have very mild linear mass dependence. We also note that the SMOM to $\overline{\text{MS}}$ matching factors are much closer to unity, suggesting a better behaved perturbative series and a reduced perturbative matching uncertainty. Therefore we strongly advocate using SMOM renormalisation conditions, which are theoretically much cleaner.

We have argued that the discrepancies from results of [13, 16, 17] come the renormalisation procedure. Because these discrepancies appear in those matrix elements affected by these issues, we suggest avoiding the RI-MOM renormalisation conditions, at least for this set of operators. [7]

Even we assess a rather conservative 5% systematic error from the renormalisation procedure in RI-MOM, our results are still not compatible with the RI-SMOM ones. It remains the possibility of a conspiracy between these infrared artefacts and omitted term in the perturbative matching. Even if the latter should be of order α_s^2, the anomalous dimensions of those operators are rather large. Since a computation at the next order is technically very challenging, this systematic error is difficult to control without using multiple schemes.

---

[7] A similar discrepancy was also recently observed in D-mixing calculations using RI-MOM [13, 36] vs. 'mostly nonperturbative' (mNPR) [37] matching.

VI. CONCLUSIONS

In this work we have defined and investigated new RI-SMOM intermediate schemes for the renormalisation of $\Delta F = 2$ four-quark operators needed for neutral kaon mixing beyond the standard model studies. These schemes can easily be generalised to other processes. We have implemented these different schemes and shown that they lead to consistent results after continuum extrapolation and conversion to $\overline{\text{MS}}$. These results are, however, inconsistent with those obtained using the intermediate RI-MOM scheme.

Although the theoretical advantages of the RI-SMOM schemes - as compared to RI-MOM - have been known for a long time, we have provided further numerical evidences in the context BSM kaon mixing:

- No pole subtraction is required.

- The chirally-forbidden matrix elements are largely suppressed.

- The Z and conversion matrices are closer to the identity matrix; the scale-evolution between 2 and 3 GeV is relatively close to the perturbative prediction (known at next-to-leading order).

On the other hand, in the RI-MOM scheme the effects of chiral symmetry breaking can be large even at large momentum, and a procedure must be used to remove infrared contributions that dominate some vertex functions in the chiral limit. We investigated the effect of different subtraction procedures in our RI-MOM data and found some dependence on the procedure, which may be at least partly responsible for the discrepancies in O_4 and O_5. These effects are particularly important in the $(S + P)$ and $(S - P)$ channels. We have shown that the RI-SMOM procedure is superior because the unwanted infrared behaviour is nearly completely suppressed (and has better pertubative behaviour).

Our study indicates these discrepancies in O_4 and O_5 could be due to a conspiracy of systematic errors in the RI-MOM scheme, the dominant ones being the infrared contamination and the truncation error of the perturbative series in the matching to $\overline{\text{MS}}$ (as these operators have rather large anomalous dimension).

In other to have a better control on the physical point extrapolation, we are currently investigating the effects of including physical pion-mass ensembles and a finer lattice spacing. Our preliminary analysis [38, 39] shows that our results are stable and we hope to decrease the un-

certainties on the BSM matrix elements by at least a factor of two. We are also investigating a strategy to run through the charm threshold with $n_f = 2 + 1 + 1$ flavours [40, 41].

ACKNOWLEDGEMENTS

VII.   APPENDICES

A.   Renormalisation of the Bag parameters

By solving numerically Eq.20, we obtained the NPR matrix Z_{ij}/Z_V^2, such that the first element $i = j = 1$ corresponds to Z_{B_K}. However, the vacuum saturation approximation of the BSM matrix elements involve the pseudo-scalar density rather than the axial current. Therefore we compute the BSM renormalisation matrix in the following way

$$\mathfrak{Z}_{ij}^{(\mathcal{A})} = \frac{Z_V^2}{Z_S^{(\mathcal{B})}} \frac{Z_{ij}^{(\mathcal{A},\mathcal{B})}}{Z_V^2} \ , \tag{44}$$

where we used the fact that $Z_S = Z_P$ in the chiral limit. The BSM bag parameters are then renormalised by

$$B_i^{(\mathcal{A})} = \mathfrak{Z}_{ij}^{(\mathcal{A})} B_j^{bare} \ , \qquad i,j \geq 2 \ . \tag{45}$$

For clarity, we note that Eq.(44) is equivalent to imposing the renormalisation condition

$$\mathfrak{Z}_{ij}^{(\mathcal{A})}(\mu,a) \left[\frac{P_k^{\mathcal{A}} \left[\Pi_j^{bare}(a,p^2) \right]}{(P_S \left[\Pi_S^{bare}(a,p^2) \right])^2} \right]_{p^2 = \mu^2} = \frac{F_{ik}^{\mathcal{A}}}{F_S^2} \ . \tag{46}$$

The factor Z_S in Eq.(44) is computed through

$$Z_S^{(\mathcal{A})} = Z_V \times \frac{P_V^{(\mathcal{A})} \left[\Pi_V \right]}{F_V^{\mathcal{A}}} \times \frac{F_S}{P_S \left[\Pi_S \right]} \ , \qquad \text{where } \mathcal{A} \in [\gamma_\mu, \rlap{/}{q}] \ . \tag{47}$$

	a_{24}	a_{32}
$F_V^{(\gamma_\mu)}/\Lambda_V^{(\gamma_\mu)}(3\text{ GeV}, a)$	0.94952(17)	0.96339(16)
$F_V^{(\not{q})}/\Lambda_V^{(\not{q})}(3\text{ GeV}, a)$	0.89737(19)	0.91410(37)
$F_S/\Lambda_S(3\text{ GeV}, a)$	0.8743(7)	0.8526(8)
$Z_V(a)$	0.71273(26)	0.74404(181)

TABLE XVI. Values used for the renormalisation factors of the bilinear needed for the BSM bag parameters.

Note that the choice $\mathcal{A} = \not{q}$ (resp. γ_μ) corresponds to the scheme called $\mathrm{RI} - \mathrm{SMOM}$ (resp. $\mathrm{RI} - \mathrm{SMOM}_{\gamma_\mu}$) in [29]. We find

$$Z_S^{(\gamma_\mu)}(3\text{ GeV}, a_{24}) = 0.6563(6), \quad Z_S^{(\not{q})}(3\text{ GeV}, a_{24}) = 0.6945(5) ,$$
$$Z_S^{(\gamma_\mu)}(3\text{ GeV}, a_{32}) = 0.6585(6), \quad Z_S^{(\not{q})}(3\text{ GeV}, a_{32}) = 0.6940(6) .$$
(48)

In order to match our results to $\overline{\mathrm{MS}}$, we also need the conversion factor for Z_S, as can seen from Eq. 44. The one-loop coefficient can extracted from [29] whereas the next-to-next-to-leading-order corrections are known from [42, 43]. Here we follow [22] and with $\alpha_s(3\text{GeV}) = 0.24544$, we find

$$R_S^{\overline{\mathrm{MS}}\leftarrow(\gamma_\mu)}(3\text{ GeV}) = 1.05259$$
$$R_S^{\overline{\mathrm{MS}}\leftarrow(\not{q})}(3\text{ GeV}) = 1.01664$$
(49)

up to α_s^3 terms. Putting everything together, we find

$$Z_S^{\overline{\mathrm{MS}}\leftarrow(\gamma_\mu)}(3\text{ GeV}, a_{24}) = 0.6908(6), \quad Z_S^{\overline{\mathrm{MS}}\leftarrow(\not{q})}(3\text{ GeV}, a_{24}) = 0.7060(6) ,$$
$$Z_S^{\overline{\mathrm{MS}}\leftarrow(\gamma_\mu)}(3\text{ GeV}, a_{32}) = 0.6931(6), \quad Z_S^{\overline{\mathrm{MS}}\leftarrow(\not{q})}(3\text{ GeV}, a_{32}) = 0.7056(6) .$$
(50)

For the reader's convenience, we report the values used in this analysis in table XVI,

For completeness, we also give Z_S at 2GeV. In the RI-SMOM schemes, we find

$$Z_S^{(\gamma_\mu)}(2\text{ GeV}, a_{24}) = 0.5974(9), \quad Z_S^{(\not{q})}(2\text{ GeV}, a_{24}) = 0.6423(8) ,$$
$$Z_S^{(\gamma_\mu)}(2\text{ GeV}, a_{32}) = 0.6585(6), \quad Z_S^{(\not{q})}(2\text{ GeV}, a_{32}) = 0.6940(6) .$$
(51)

With $\alpha_s(2\text{Gev}) = 0.2961$, the conversion factors read

$$R_S^{\overline{\mathrm{MS}}\leftarrow(\gamma_\mu)}(2\text{ GeV}) = 1.06689 ,$$
$$R_S^{\overline{\mathrm{MS}}\leftarrow(\not{q})}(2\text{ GeV}) = 1.02107 ,$$
(52)

therefore

$$Z_S^{\overline{\mathrm{MS}}\leftarrow(\gamma_\mu)}(2\text{ GeV}, a_{24}) = 0.5924(14), \quad Z_S^{\overline{\mathrm{MS}}\leftarrow(\not{q})}(2\text{ GeV}, a_{24}) = 0.6372(17) ,$$
$$Z_S^{\overline{\mathrm{MS}}\leftarrow(\gamma_\mu)}(2\text{ GeV}, a_{32}) = 0.6320(15), \quad Z_S^{\overline{\mathrm{MS}}\leftarrow(\not{q})}(2\text{ GeV}, a_{32}) = 0.6506(17) .$$
(53)

B. Matching factors between the RI-SMOM schemes and $\overline{\text{MS}}$

The conversion between the RI-SMOM schemes and $\overline{\text{MS}}$ (of [6]) is given at one-loop order. We define (we chose a negative sign for historical reasons)

$$R^{\overline{\text{MS}}\leftarrow\text{scheme}} = 1 - \frac{\alpha_s}{4\pi} \Delta r^{\overline{\text{MS}}\leftarrow\text{scheme}} . \tag{54}$$

In the following expressions, the constant C_0 is $C_0 = \frac{2\psi^{(1)}\left(\frac{1}{3}\right)}{3} - \left(\frac{2\pi}{3}\right)^2$, where ψ is the PolyGamma function, N is the number of colors and ξ the usual gauge parameter (the non-perturbative Z-factors have been computed in the Landau gauge, $\xi = 0$). Note that the coefficients for the $(27, 1)$ and the $(8, 8)$ operators were already known or could be derived from [31, 33]. The others are new, they have been computed for this work. First we have the matching factors for the (γ_μ, γ_μ) scheme, for the $(27, 1)$ operator we have

$$\Delta r_{11}^{\overline{\text{MS}}\leftarrow(\gamma_\mu,\gamma_\mu)} = -\frac{8}{N} + \frac{12\log(2)}{N} + 8 - 12\log(2) + \xi \left(-\frac{C_0}{2N} + \frac{C_0}{2} - \frac{1}{2N} + \frac{4\log(2)}{N} + \frac{1}{2} - 4\log(2) \right) , \tag{55}$$

For the $(8, 8)$ doublet:

$$\Delta r_{22}^{\overline{\text{MS}}\leftarrow(\gamma_\mu,\gamma_\mu)} = -\frac{3C_0}{2N} + \frac{2}{N} + \frac{2\log(2)}{N} + \xi \left(-\frac{C_0}{2N} + \frac{1}{2N} + \frac{2\log(2)}{N} \right) ,$$

$$\Delta r_{23}^{\overline{\text{MS}}\leftarrow(\gamma_\mu,\gamma_\mu)} = -3C_0 + 4 + 4\log(2) + \xi \left(-C_0 + 1 + 4\log(2) \right) ,$$

$$\Delta r_{32}^{\overline{\text{MS}}\leftarrow(\gamma_\mu,\gamma_\mu)} = \log(2) - \frac{3}{2} + \xi \left(\log(2) - \frac{C_0}{4} \right) , \tag{56}$$

$$\Delta r_{33}^{\overline{\text{MS}}\leftarrow(\gamma_\mu,\gamma_\mu)} = \frac{3C_0 N}{2} - \frac{3C_0}{2N} - 5N + \frac{2}{N} + \frac{2\log(2)}{N} + \xi \left(-\frac{C_0}{2N} - \frac{N}{2} + \frac{1}{2N} + \frac{2\log(2)}{N} \right) ,$$

and for the $(6, \bar{6})$ doublet:

$$\Delta r_{44}^{\overline{\text{MS}}\leftarrow(\gamma_\mu,\gamma_\mu)} = \frac{3C_0 N}{2} - \frac{3C_0}{2N} - \frac{3C_0}{4} - 5N + \frac{5}{N} + \frac{2\log(2)}{N} + 7 - 4\log(2)$$
$$+ \xi \left(-\frac{C_0}{2N} - \frac{C_0}{4} - \frac{N}{2} + \frac{1}{2N} + \frac{2\log(2)}{N} + \frac{1}{2} \right) ,$$

$$\Delta r_{45}^{\overline{\text{MS}}\leftarrow(\gamma_\mu,\gamma_\mu)} = 4 \left(\frac{C_0}{8N} - \frac{C_0}{16} - \frac{7}{6N} + \frac{5\log(2)}{6N} + \frac{7}{12} - \frac{2\log(2)}{3} \right)$$
$$+ 4\xi \left(\frac{C_0}{16} - \frac{1}{12N} + \frac{\log(2)}{6N} + \frac{1}{24} - \frac{\log(2)}{3} \right) , \tag{57}$$

$$\Delta r_{54}^{\overline{\text{MS}}\leftarrow(\gamma_\mu,\gamma_\mu)} = \frac{1}{4} \left(\frac{6C_0}{N} + 9C_0 - \frac{16}{N} + \frac{40\log(2)}{N} + 4 - 32\log(2) \right)$$
$$+ \frac{1}{4}\xi \left(3C_0 - \frac{4}{N} + \frac{8\log(2)}{N} - 2 - 16\log(2) \right) ,$$

$$\Delta r_{55}^{\overline{\text{MS}}\leftarrow(\gamma_\mu,\gamma_\mu)} = -\frac{C_0 N}{2} - \frac{C_0}{2N} - \frac{C_0}{4} + \frac{N}{3} - \frac{7}{3N} + \frac{26\log(2)}{3N} + 3 - \frac{28\log(2)}{3}$$
$$+ \xi \left(-\frac{C_0}{2N} + \frac{C_0}{4} + \frac{N}{6} - \frac{1}{6N} + \frac{10\log(2)}{3N} + \frac{1}{2} - \frac{8\log(2)}{3} \right) .$$

Secondly are the matching factors to $\overline{\text{MS}}$ of the $(\slashed{q}, \slashed{q})$ scheme, the $(27, 1)$ is

$$\Delta r_{11}^{\overline{\text{MS}} \leftarrow (\slashed{q}, \slashed{q})} = -\frac{9}{N} + \frac{12 \log(2)}{N} + 9 - 12 \log(2) + \xi \left(-\frac{C_0}{N} + C_0 + \frac{4 \log(2)}{N} - 4 \log(2) \right) . \tag{58}$$

For the $(8, 8)$ doublet we have

$$\Delta r_{22}^{\overline{\text{MS}} \leftarrow (\slashed{q}, \slashed{q})} = -\frac{3 C_0}{2N} + \frac{2}{N} + \frac{2 \log(2)}{N} + \xi \left(-\frac{C_0}{2N} + \frac{1}{2N} + \frac{2 \log(2)}{N} \right) ,$$

$$\Delta r_{23}^{\overline{\text{MS}} \leftarrow (\slashed{q}, \slashed{q})} = -3 C_0 + 4 + 4 \log(2) + \xi \left(-C_0 + 1 + 4 \log(2) \right) ,$$

$$\Delta r_{32}^{\overline{\text{MS}} \leftarrow (\slashed{q}, \slashed{q})} = \log(2) - 1 + \xi \left(\log(2) - \frac{1}{4} \right) ,$$

$$\Delta r_{33}^{\overline{\text{MS}} \leftarrow (\slashed{q}, \slashed{q})} = \frac{3 C_0 N}{2} - \frac{3 C_0}{2N} - 4N + \frac{2}{N} + \frac{2 \log(2)}{N} + \xi \left(\frac{C_0 N}{2} - \frac{C_0}{2N} - N + \frac{1}{2N} + \frac{2 \log(2)}{N} \right) , \tag{59}$$

and for the $(6, \bar{6})$ doublet:

$$\Delta r_{44}^{\overline{\text{MS}} \leftarrow (\slashed{q}, \slashed{q})} = \frac{3 C_0 N}{2} - \frac{C_0}{N} - \frac{C_0}{4} - 4N + \frac{3}{N} + \frac{2 \log(2)}{N} + 6 - 4 \log(2)$$
$$+ \xi \left(\frac{C_0 N}{2} - \frac{3 C_0}{2N} - \frac{3 C_0}{4} - N + \frac{2}{N} + \frac{2 \log(2)}{N} + \frac{3}{2} \right) ,$$

$$\Delta r_{45}^{\overline{\text{MS}} \leftarrow (\slashed{q}, \slashed{q})} = 4 \left(\frac{C_0}{12 N} - \frac{5 C_0}{48} - \frac{13}{12 N} + \frac{5 \log(2)}{6N} + \frac{2}{3} - \frac{2 \log(2)}{3} \right)$$
$$+ 4 \xi \left(\frac{C_0}{24 N} + \frac{5 C_0}{48} - \frac{1}{6N} + \frac{\log(2)}{6N} - \frac{1}{24} - \frac{\log(2)}{3} \right) ,$$

$$\Delta r_{54}^{\overline{\text{MS}} \leftarrow (\slashed{q}, \slashed{q})} = \frac{1}{4} \left(4 C_0 N + \frac{4 C_0}{N} + 11 C_0 - 8N - \frac{12}{N} + \frac{40 \log(2)}{N} - 32 \log(2) \right)$$
$$+ \frac{1}{4} \xi \left(-4 C_0 N + \frac{2 C_0}{N} + C_0 + 8N - \frac{8}{N} + \frac{8 \log(2)}{N} + 2 - 16 \log(2) \right) , \tag{60}$$

$$\Delta r_{55}^{\overline{\text{MS}} \leftarrow (\slashed{q}, \slashed{q})} = -\frac{5 C_0 N}{6} - \frac{C_0}{3N} - \frac{5 C_0}{12} + 2N - \frac{11}{3N} + \frac{26 \log(2)}{3N} + \frac{10}{3} - \frac{28 \log(2)}{3}$$
$$+ \xi \left(\frac{5 C_0 N}{6} - \frac{7 C_0}{6N} + \frac{5 C_0}{12} - N + \frac{2}{3N} + \frac{10 \log(2)}{3N} + \frac{1}{6} - \frac{8 \log(2)}{3} \right) .$$

The factors for other schemes can be obtained trivially if ones knows for example the matching coefficients for the SM operator

$$\Delta r_{11}^{\overline{\text{MS}} \leftarrow (\gamma_\mu, \slashed{q})} = N - \frac{9}{N} + \frac{12 \log(2)}{N} + 8 - 12 \log(2)$$
$$+ \xi \left(\frac{C_0 N}{2} - \frac{C_0}{N} + \frac{C_0}{2} - \frac{N}{2} + \frac{4 \log(2)}{N} + \frac{1}{2} - 4 \log(2) \right) , \tag{61}$$

from which we can derive

$$\Delta r_{11}^{\overline{\text{MS}} \leftarrow (\slashed{q}, \gamma_\mu)} = -N - \frac{8}{N} + \frac{12 \log(2)}{N} + 9 - 12 \log(2)$$
$$+ \xi \left(-\frac{C_0 N}{2} - \frac{C_0}{2N} + C_0 + \frac{N}{2} - \frac{1}{2N} + \frac{4 \log(2)}{N} - 4 \log(2) \right) . \tag{62}$$

Although they can be obtained from the the previous equations, for completeness we also list the other matching factors for the $(\not q, \gamma_\mu)$ sheme. For the $(8,8)$ doublet:

$$\Delta r_{22}^{\overline{\text{MS}} \leftarrow (\not q, \gamma_\mu)} = -\frac{3C_0}{2N} - N + \frac{3}{N} + \frac{2\log(2)}{N} + \xi\left(-\frac{C_0 N}{2} + \frac{N}{2} + \frac{2\log(2)}{N}\right),$$

$$\Delta r_{23}^{\overline{\text{MS}} \leftarrow (\not q, \gamma_\mu)} = -3C_0 + 4 + 4\log(2) + \xi\left(-C_0 + 1 + 4\log(2)\right),$$

$$\Delta r_{32}^{\overline{\text{MS}} \leftarrow (\not q, \gamma_\mu)} = -1 + \log(2) + \xi\left(\log(2) - \frac{1}{4}\right),$$

$$\Delta r_{33}^{\overline{\text{MS}} \leftarrow (\not q, \gamma_\mu)} = \frac{3C_0 N}{2} - \frac{3C_0}{2N} - 5N + \frac{3}{N} + \frac{2\log(2)}{N} + \xi\left(\frac{2\log(2)}{N} - \frac{N}{2}\right),$$

(63)

and finally for the $(6, \bar 6)$ doublet:

$$\Delta r_{44}^{\overline{\text{MS}} \leftarrow (\not q, \gamma_\mu)} = \frac{3C_0 N}{2} - \frac{C_0}{N} - \frac{C_0}{4} - 5N + \frac{4}{N} + \frac{2\log(2)}{N} + 6 - 4\log(2)$$
$$+ \xi\left(-\frac{C_0}{N} - \frac{3C_0}{4} - \frac{N}{2} + \frac{3}{2N} + \frac{2\log(2)}{N} + \frac{3}{2}\right),$$

$$\Delta r_{45}^{\overline{\text{MS}} \leftarrow (\not q, \gamma_\mu)} = 4\left(\frac{C_0}{12N} - \frac{5C_0}{48} - \frac{13}{12N} + \frac{5\log(2)}{6N} + \frac{2}{3} - \frac{2\log(2)}{3}\right)$$
$$+ 4\xi\left(\frac{C_0}{24N} + \frac{5C_0}{48} - \frac{1}{6N} + \frac{\log(2)}{6N} - \frac{1}{24} - \frac{\log(2)}{3}\right),$$

$$\Delta r_{54}^{\overline{\text{MS}} \leftarrow (\not q, \gamma_\mu)} = \frac{1}{4}\left(4C_0 N + \frac{4C_0}{N} + 11C_0 - 8N - \frac{12}{N} + \frac{40\log(2)}{N} - 32\log(2)\right)$$
$$+ \frac{1}{4}\xi\left(-4C_0 N + \frac{2C_0}{N} + C_0 + 8N - \frac{8}{N} + \frac{8\log(2)}{N} + 2 - 16\log(2)\right),$$

$$\Delta r_{55}^{\overline{\text{MS}} \leftarrow (\not q, \gamma_\mu)} = -\frac{5C_0 N}{6} - \frac{C_0}{3N} - \frac{5C_0}{12} + N - \frac{8}{3N} + \frac{26\log(2)}{3N} + \frac{10}{3} - \frac{28\log(2)}{3}$$
$$+ \xi\left(\frac{C_0 N}{3} - \frac{2C_0}{3N} + \frac{5C_0}{12} - \frac{N}{2} + \frac{1}{6N} + \frac{10\log(2)}{3N} + \frac{1}{6} - \frac{8\log(2)}{3}\right).$$

(64)

C. Figures for the non-perturbative running

In Fig 7 we show the running between $\mu_1 = 2\,\text{GeV}$ and μ where μ varies between $2\,\text{GeV}$ and 3GeV.

We divide the non-perturbative running by the perturbative expectation, ie we compute

$$\sigma(\mu_1, \mu_2) U(\mu_1, \mu_2)^{-1}$$

(65)

where $\mu_1 = \mu$ varies between 2 and $3\,\text{GeV}$, while $\mu_2 = 3\,\text{GeV}$ is fixed. U is the same running computed either at leading order or at next-to-leading in perturbation theory. The results are shown in Figs. 11.

We observe the running can be relatively important, see for example σ_{33} and σ_{44}, this is expected from their anomalous dimension [4–6] . Starting from $\mu = 3$ GeV and running down to 2 GeV, the
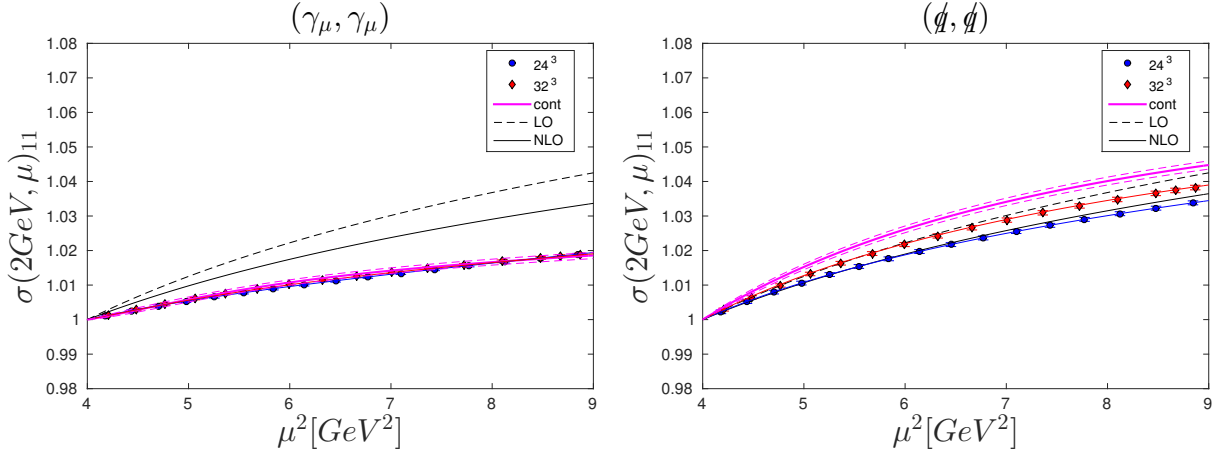
FIG. 7. Scale evolution of the $(27,1)$ operator for the various schemes; left: (γ_μ, γ_μ), right: $(\slashed{q}, \slashed{q})$. We show the non-perturbative running computed on the coarse lattice, on the fine lattice and extrapolated to the continuum. We also compare with the perturbative prediction at leading-order (LO) and next-to-leading-order (NLO).

non-perturbative scale evolution is qualitatively well-described by the Next-to-Leading perturbative prediction. In the worse cases we observe a deviation of around 5 % at 2 GeV. In a future we will include a finer lattice spacing to have a better handle on the discretisation effects.
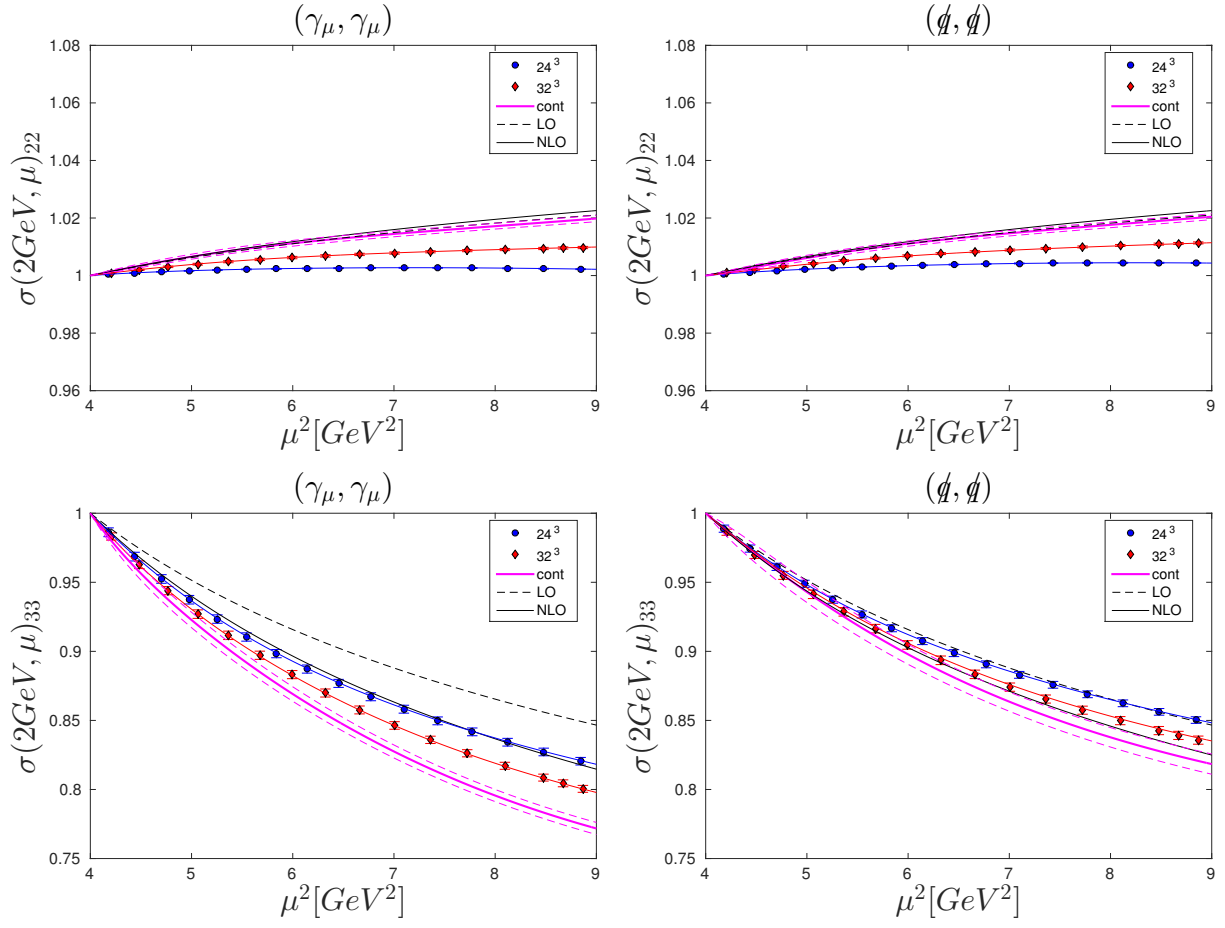
FIG. 8. Same as the previous plot for the scale evolution of the diagonal $(8, 8)$ mixing matrix element σ_{22} and σ_{33}.
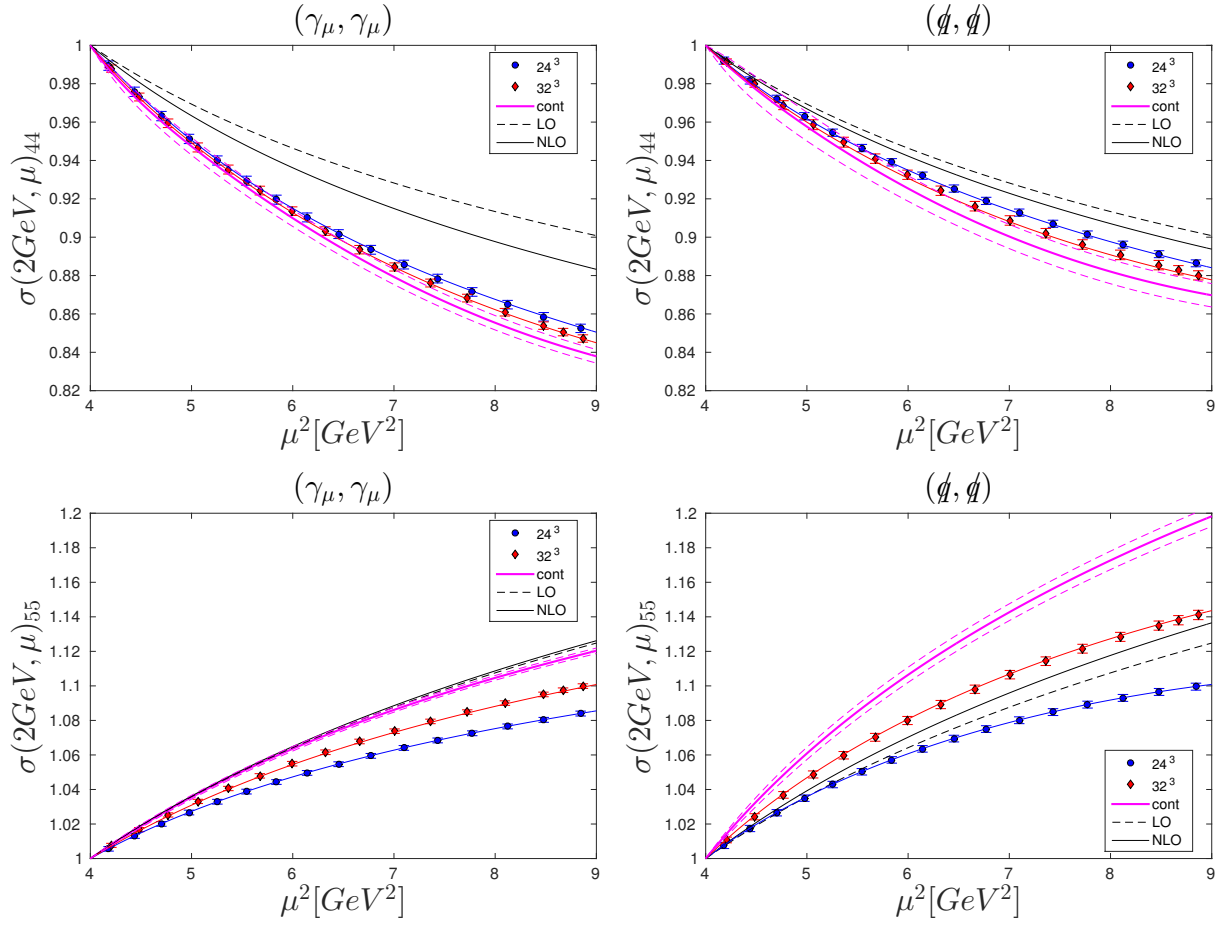
FIG. 9. Same as the previous plot for the scale evolution of the diagonal $(6, \bar{6})$ mixing matrix element σ_{44} and σ_{55}.
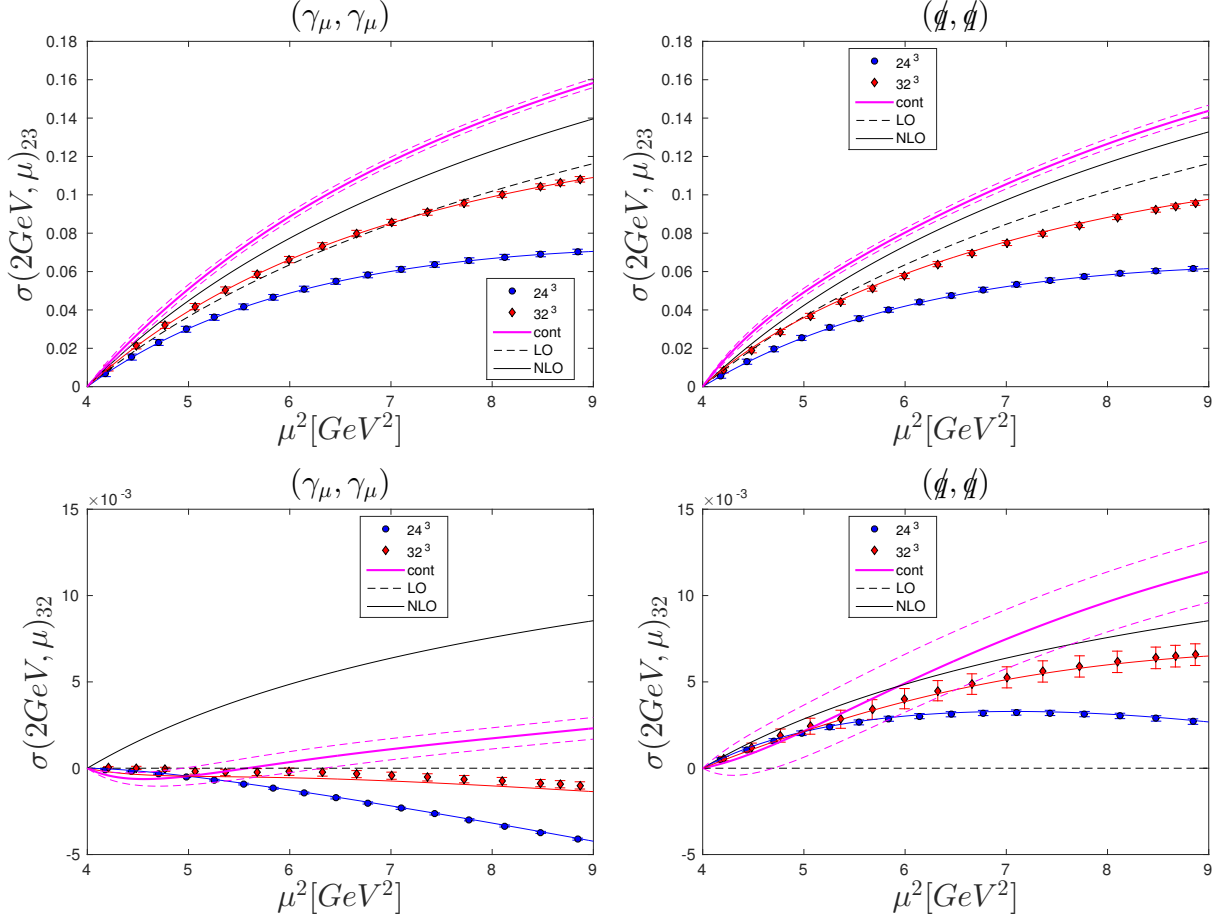
FIG. 10. Same as the previous plot for the scale evolution of the non-diagonal $(8, 8)$ mixing matrix element σ_{32} and σ_{33}.
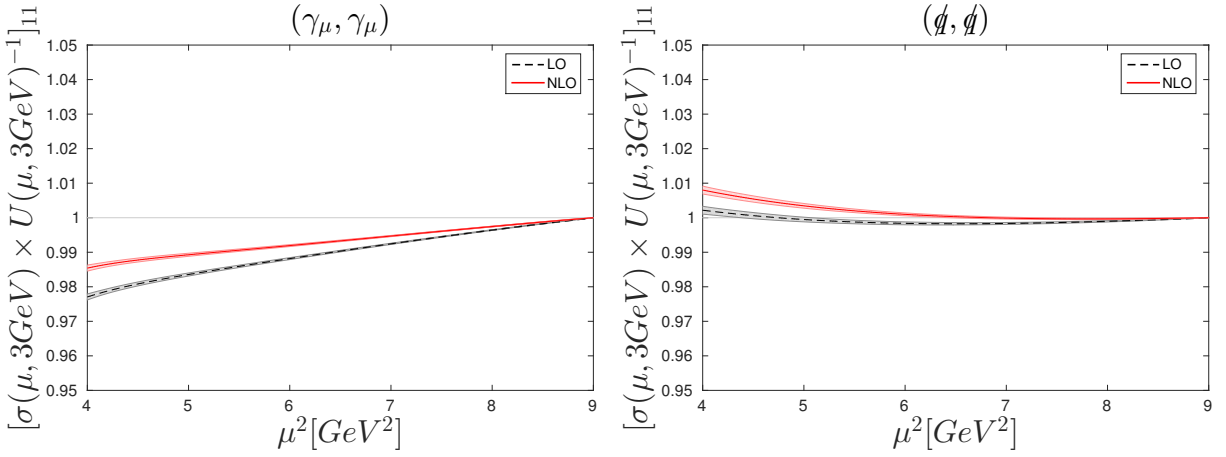

FIG. 11. Ratio $\sigma(\mu, 3\text{GeV}) \times U(\mu, 3\text{GeV})^{-1}$ for the $(27, 1)$ operator and for the various schemes; left: (γ_μ, γ_μ), right: $(\not{q}, \not{q})$.
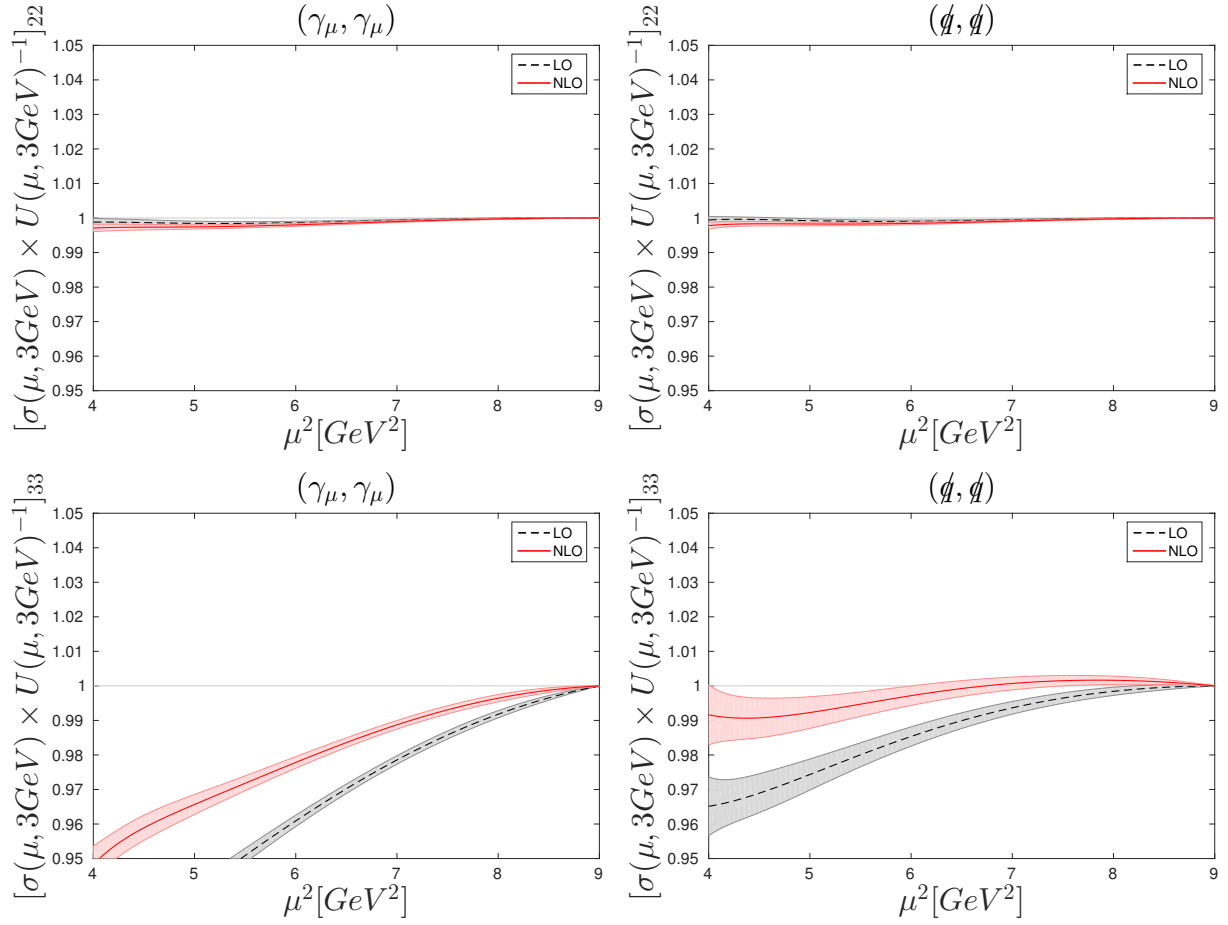
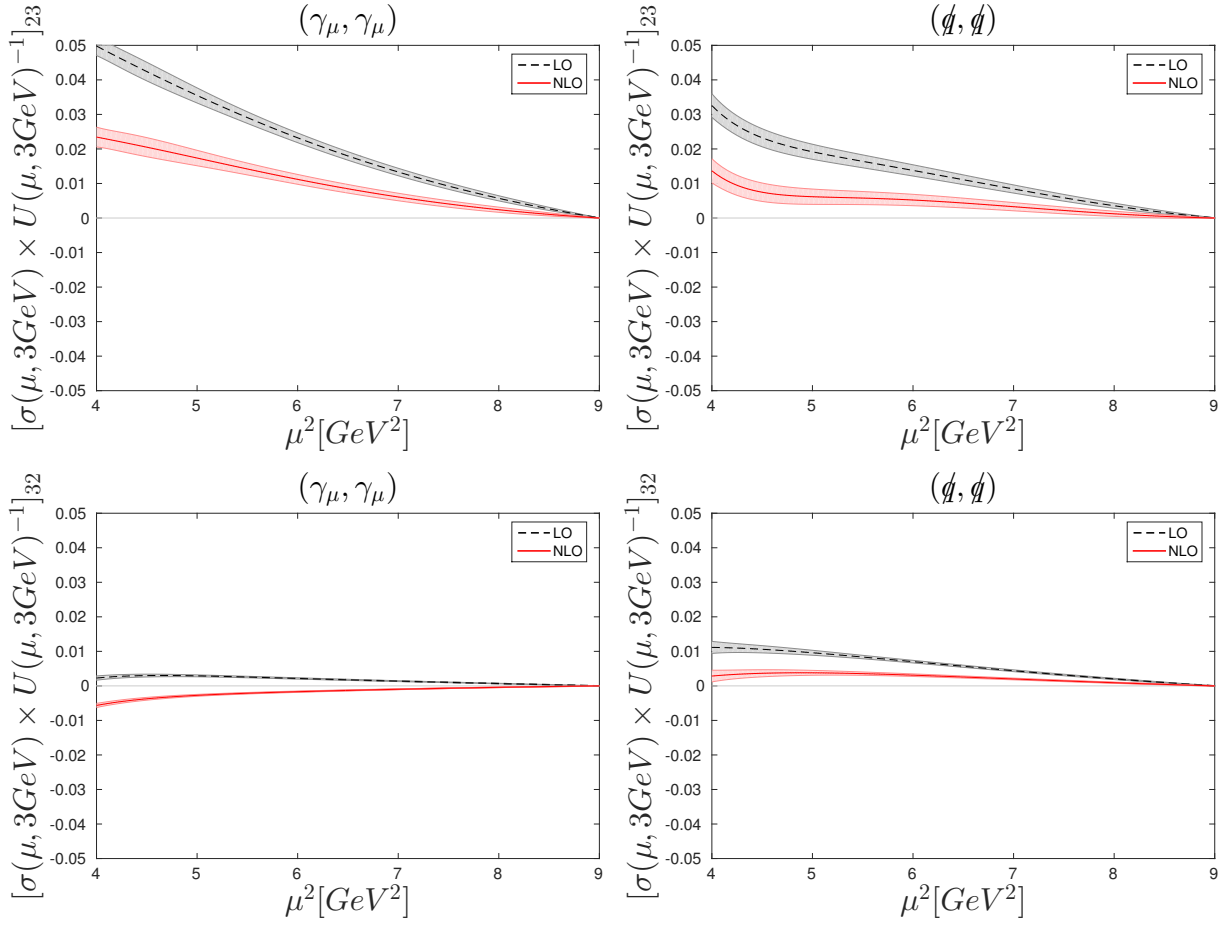FIG. 12. Same as the previous plot for the diagonal $(8,8)$ mixing matrix element.

FIG. 13. Same as the previous plot for the off-diagonal $(8, 8)$ mixing matrix element.
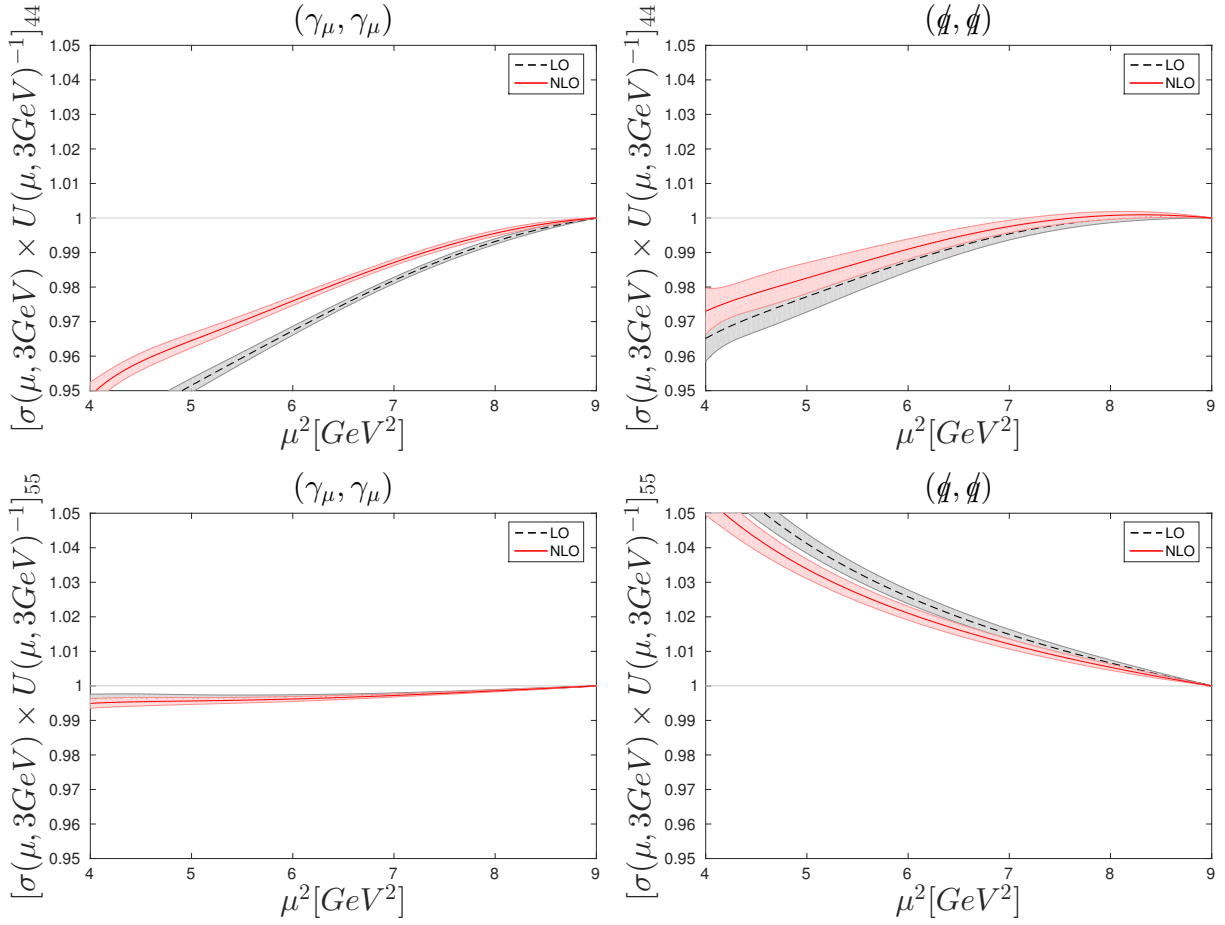
FIG. 14. Same as the previous plot for the diagonal $(6, \bar{6})$ mixing matrix element.

D. Fierz relations

In Eq.(7), we have only considered four-quark operators with a colour-unmixed structure

$$(\bar{s}_a\Gamma d_a)(\bar{s}_b\Gamma d_b) \equiv (\bar{s}\Gamma d)(\bar{s}\Gamma d)_{\mathrm{unm}} \tag{66}$$

However the color partners

$$(\bar{s}_a\Gamma d_b)(\bar{s}_b\Gamma d_a) \equiv (\bar{s}\Gamma d)(\bar{s}\Gamma d)_{\mathrm{mix}} \tag{67}$$

can be recovered by a Fierz transformation,

$$Q_i^{\mathrm{mix}} = F_{ij}Q_j^{\mathrm{unm}} \,, \tag{68}$$

that we give explicitly here. For the dirac structure, we introduce the standard notation

$$
\begin{aligned}
SS &= (\bar{s}d)(\bar{s}d) \,, \\
VV &= (\bar{s}\gamma_\mu d)(\bar{s}\gamma_\mu d) \,, \\
TT &= \sum_{\nu>\mu}(\bar{s}\gamma_\mu\gamma_\nu d)(\bar{s}\gamma_\mu\gamma_\nu d) \,, \\
AA &= (\bar{s}\gamma_\mu\gamma_5 d)(\bar{s}\gamma_\mu\gamma_5 d) \,, \\
PP &= (\bar{s}\gamma_5 d)(\bar{s}\gamma_5 d) \,.
\end{aligned}
\tag{69}
$$

For Euclidean γ matrices the Fierz transformation in the NPR basis reads

$$
\begin{pmatrix} VV+AA \\ VV-AA \\ SS-PP \\ SS+PP \\ TT \end{pmatrix}_{\mathrm{(mix)}}
=
\begin{pmatrix}
1 & 0 & 0 & 0 & 0 \\
0 & 0 & -2 & 0 & 0 \\
0 & -1/2 & 0 & 0 & 0 \\
0 & 0 & 0 & -1/2 & 1/2 \\
0 & 0 & 0 & 3/2 & 1/2
\end{pmatrix}
\times
\begin{pmatrix} VV+AA \\ VV-AA \\ SS-PP \\ SS+PP \\ TT \end{pmatrix}_{\mathrm{(unm)}}
\tag{70}
$$

Results in the literature are often given in the SUSY basis [44–46], which was also our choice in [1],

$$
\begin{aligned}
O_2 &= (\bar{s}_a(1-\gamma_5)d_a)\,(\bar{s}_b(1-\gamma_5)d_b) \\
O_3 &= (\bar{s}_a(1-\gamma_5)d_b)\,(\bar{s}_b(1-\gamma_5)d_a) \\
O_4 &= (\bar{s}_a(1-\gamma_5)d_a)\,(\bar{s}_b(1+\gamma_5)d_b) \\
O_5 &= (\bar{s}_a(1-\gamma_5)d_b)\,(\bar{s}_b(1+\gamma_5)d_a) \,,
\end{aligned}
\tag{71}
$$

in addition to $O_1 = Q_1$. In practice we only consider the parity even part of these operators. The relation between the NPR and the SUSY basis is then given by $O^+ = TQ^+$ where

$$
T = \begin{pmatrix}
1 & 0 & 0 & 0 & 0 \\
0 & 0 & 0 & 1 & 0 \\
0 & 0 & 0 & -1/2 & 1/2 \\
0 & 0 & 1 & 0 & 0 \\
0 & -1/2 & 0 & 0 & 0
\end{pmatrix} . \tag{72}
$$

[1] RBC/UKQCD, N. Garron, R.J. Hudspith and A.T. Lytle, JHEP 11 (2016) 001, 1609.03334.

[2] G. Martinelli et al., Nucl. Phys. B445 (1995) 81, hep-lat/9411010.

[3] P.V. Mainar, M. Dalla Brida and M. Papinutto, PoS LATTICE2015 (2016) 252.

[4] M. Papinutto, C. Pena and D. Preti, Eur. Phys. J. C77 (2017) 376, 1612.06461.

[5] M. Ciuchini et al., Nucl.Phys. B523 (1998) 501, hep-ph/9711402.

[6] A.J. Buras, M. Misiak and J. Urban, Nucl.Phys. B586 (2000) 397, hep-ph/0005183.

[7] RBC/UKQCD, R. Arthur and P. Boyle, Phys.Rev. D83 (2011) 114511, 1006.0422.

[8] RBC/UKQCD, R. Arthur et al., Phys.Rev. D85 (2012) 014501, 1109.1223.

[9] M. Gockeler et al., Nucl.Phys. B544 (1999) 699, hep-lat/9807044.

[10] P.F. Bedaque, Phys. Lett. B593 (2004) 82, nucl-th/0402051.

[11] G.M. de Divitiis, R. Petronzio and N. Tantalo, Phys. Lett. B595 (2004) 408, hep-lat/0405002.

[12] C.T. Sachrajda and G. Villadoro, Phys. Lett. B609 (2005) 73, hep-lat/0411033.

[13] ETM, N. Carrasco et al., Phys. Rev. D92 (2015) 034516, 1505.06639.

[14] SWME, T. Bae et al., Phys.Rev. D88 (2013) 071503, 1309.2040.

[15] SWME, Y.C. Jang et al., (2015), 1509.00592.

[16] RBC/UKQCD, P. Boyle, N. Garron and R. Hudspith, Phys.Rev. D86 (2012) 054028, 1206.5737.

[17] ETM, V. Bertone et al., JHEP 03 (2013) 089, 1207.1287, [Erratum: JHEP07,143(2013)].

[18] R.J. Hudspith, N. Garron and A.T. Lytle, 2015, 1512.05398.

[19] R. Babich et al., Phys.Rev. D74 (2006) 073009, hep-lat/0605016.

[20] RBC/UKQCD, P. Boyle, N. Garron and A. Lytle, PoS LATTICE2011 (2011) 227, 1112.0537.

[21] P. Boyle and N. Garron, PoS LATTICE2010 (2010) 307, 1101.5579.

[22] RBC/UKQCD, R. Arthur et al., Phys.Rev. D87 (2013) 094514, 1208.4412.

[23] N. Garron et al., PoS LATTICE2012 (2012) 108, 1212.2871.

[24] RBC/UKQCD, A.T. Lytle et al., PoS LATTICE2013 (2014) 400, 1311.0322.

[25] T. Blum et al., Phys. Rev. D86 (2012) 074513, 1206.5142.

[26] T. Blum et al., Phys.Rev.Lett. 108 (2012) 141601, 1111.1699.

[27] T. Blum et al., Phys. Rev. D91 (2015) 074502, 1502.00263.

[28] Y. Aoki et al., Phys. Rev. D78 (2008) 054510, 0712.1061.

[29] C. Sturm et al., Phys.Rev. D80 (2009) 014501, 0901.2599.

[30] RBC/UKQCD, T. Blum et al., (2014), 1411.7017.

[31] Y. Aoki et al., Phys.Rev. D84 (2011) 014503, 1012.4178.

[32] M. Ciuchini et al., Nucl.Phys. B415 (1994) 403, hep-ph/9304257.

[33] C. Lehner and C. Sturm, Phys.Rev. D84 (2011) 014001, 1104.4948.

[34] T. van Ritbergen, J. Vermaseren and S. Larin, Phys.Lett. B400 (1997) 379, hep-ph/9701390.

[35] K. Chetyrkin, B.A. Kniehl and M. Steinhauser, Phys.Rev.Lett. 79 (1997) 2184, hep-ph/9706430.

[36] N. Carrasco et al., Phys. Rev. D90 (2014) 014502, 1403.7302.

[37] A. Bazavov et al., (2017), 1706.04622.

[38] RBC/UKQCD, J. Kettle et al., PoS LATTICE2016 (2016) 397, 1703.00392.

[39] RBC/UKQCD, J. Kettle et al., to appear in the roceedings LATTICE2017 (2017).

[40] RBC/UKQCD, J. Frison, P. Boyle and N. Garron, PoS LATTICE2014 (2015) 285, 1412.0834.

[41] RBC/UKQCD, J. Frison, P. Boyle and N. Garron, PoS LATTICE2015 (2016) 262, 1510.09114.

[42] M. Gorbahn and S. Jager, Phys. Rev. D82 (2010) 114001, 1004.3997.

[43] L.G. Almeida and C. Sturm, Phys. Rev. D82 (2010) 054017, 1004.4613.

[44] F. Gabbiani et al., Nucl.Phys. B477 (1996) 321, hep-ph/9604387.

[45] C. Allton et al., Phys.Lett. B453 (1999) 30, hep-lat/9806016.

[46] M. Ciuchini et al., JHEP 9810 (1998) 008, hep-ph/9808328.